MSUCL-359
August 1981

INTERMEDIATE ENERGY HEAVY ION COLLISIONS

David K. SCOTT

National Superconducting Cyclotron Laboratory

and

Departments of Physics and Chemistry
Michigan State University
East Lansing, Michigan 48824, USA

Abstract: Intermediate energy nuclear collisions between 20 and 200 MeV/nucleon are discussed. Various transitional phenomena occur in this region which acts as a bridge between low energy and relativistic heavy-ion reactions. The change from mean field to hydrodynamical phenomena, the onset of the participant-spectator description, and of high multiplicity events are all likely to be accessible at intermediate energies. The study of heavy fragments in peripheral reactions to measure zero point motion, and of light particle emission to probe properties of the participant zone in more central collisions are discussed. Exotic aspects of explosion, entropy production, of phase transitions and of nuclei far from stability can also be investigated at intermediate energies.

1. Introduction

The subject of intermediate energy, heavy-ion collisions has so far enjoyed a symbiotic relationship with its low and high energy hosts, drawing liberally from both. The reasons are partly practical and partly philosophical. Largely as a result of developments in accelerator technology, the study of nuclear collisions has been concentrated on two decades of incident energy: from 1 to 20 MeV/ nucleon by the numerous electrostatic and cyclotron accelerators throughout the world, and from 200 to 3600 MeV/nucleon by modifications to existing synchrotrons. By driving these accelerators to their high and low energy limits, some initial results in the intermediate energy regime from 20 to 200 MeV/nucleon are now available.[1-5] In like fashion, the theoretical interpretations are mainly extrapolations of ideas developed at much lower and higher energies. However the major emphasis of the new accelerators coming into operation in the next few years will be on nuclear collisions at intermediate energies, which are now known to contain important transitional features. Within the span from 20 to 200 MeV/nucleon, several thresholds can be surpassed, for example at the sound velocity, the Fermi energy and the pion mass. Instead of a mean field description, one may find that the mean free path becomes short before nuclei lose their cohesiveness; hydrodynamic features may therefore come into play. From the perspective of general physics, the region is also very interesting because of the lack of relevant, small, characteristic parameters. The situation is neither classical nor quantal, neither in the one-body nor the two-body extreme, neither close to the adiabatic nor to the sudden approximation; the energy is neither so low that the interaction might be dominated by the mean field, nor so high that individual few nucleon collisions might make the major contribution. This paper will deal with our present knowledge of intermediate energy, heavy-ion collisions and their relation to phenomena at low and at relativistic energies.

2. A general perspective

Below 10 MeV/nucleon, heavy-ion collisions have led to the discovery of the novel reaction process, deeply-inelastic scattering. In this phenomenon, nuclei behave like extended objects with a short range interaction, i.e. like sticky balls. At such low energies the duration of the collision is much longer than the transit time of a nucleon at the Fermi level. The whole nucleus therefore responds coherently to the collision and the dominant phenomena are characteristic of the mean field. In the high energy regime, the opposite could be expected to hold true. Nucleons undergo such violent collisions with each other that the reactions proceed by independent collisions of the constituent particles. An upper boundary for this description is set by allowing the two nuclei to be completely disjunct in momentum space. Since the Fermi sphere has a radius of the order 1.34 fm^{-1}, an upper limit on the required projectile energy, (for an equal mass target and projectile) is 150 MeV/nucleon. According to measurements of the reaction cross section, σ_R, it seems that the transition sets in much earlier.[6])

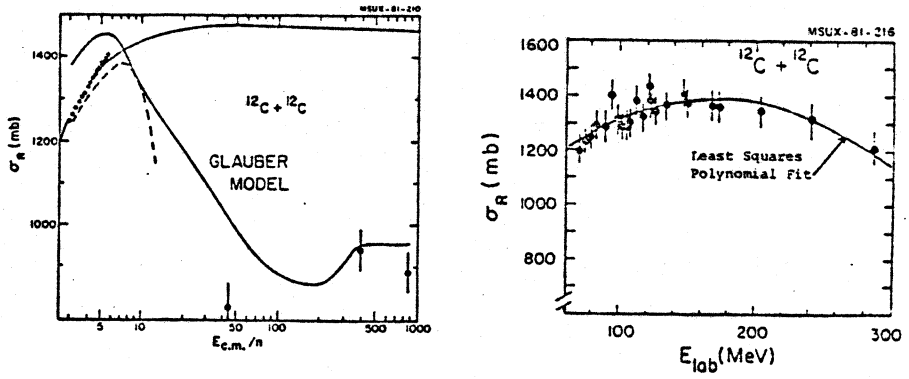

Fig. 1 Reaction cross section as a function of energy for $^{12}C + ^{12}C$ (left). The data corresponding to the dashed line are also shown (right).

The most naive expectation for σ_R is that it equals the geometrical limit, $\pi R^2(1-V/E_{cm})$, where R is the strong interaction radius, E_{cm} the center of mass energy and V is the barrier height; this limit is shown in Fig. 1 (top) for $^{12}C+^{12}C$ as a function of E_{cm}/n. (Note that n is here the number of nucleons in the projectile, and therefore the quantity E_{cm}/n is not a particularly significant parameter.) On the right are shown recent measurements[7]) at low energies from fitting the elastic scattering cross section, which suggest that the cross section begins to drop below the geometric value at an energy per nucleon of 15 MeV. The least squares polynomial fit to the data is shown in the top figure by the dashed line. The drop below the geometrical limit appears to be substantiated by higher energy data at 86,[2])

800 and 2000 MeV/nucleon.[8]) (These points appear on the plot at E_{cm}/n = 43, 400 and 1000.) The overall trends of the data are in fact rather similar to the behavior of the nucleon-nucleon total cross section, and fall even more steeply than the prediction of the Glauber model (solid line) which uses as input the nucleon-nucleon data.[6]) Alternatively the data can be parameterized with the formula:

$$\sigma_R = \pi(R+\lambda\!\!\!^{-})^2 \left(1-\frac{zZe^2}{(R+\lambda\!\!\!^{-})E_{cm}}\right) (1-T).$$

Here T is the nuclear transparency, which in the above case may be as high as 50%. These observations are taken to imply the dominance of nucleon-nucleon collisions above about 15 MeV/nucleon. It should be noted, however, that this transparency may be confined to the surface region, and that the centre of the nucleus is still black. Taking the $^{12}C+^{12}C$ strong interaction radius as

$$r_o (A_1^{1/3} + A_2^{1/3} - \delta),$$

then δ of only 1.3 fm accounts for a 50% transparency. Further discussions of the effects in nucleus-nucleus reaction cross sections are given in ref. 4.

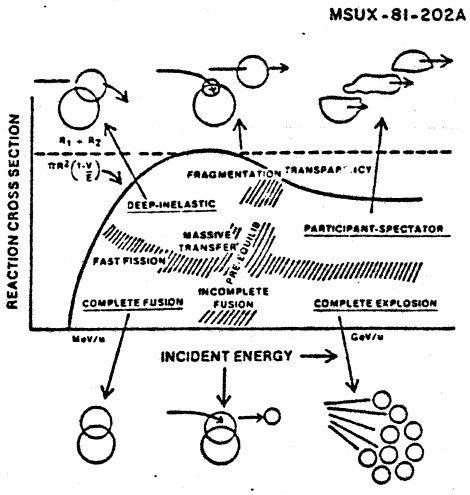

Fig. 2 Schematic illustration of nuclear collisions as a function of impact parameter and energy/nucleon.

Although the results suggest a change in the nature of heavy-ion collisions above 15 MeV/nucleon, the immediate conclusion should not be that only trivial processes take place at higher energies. Some of the known interesting processes are indicated schematically[1]) in Fig. 2 as a function of incident energy and impact parameter for a typical system like ^{40}Ar on ^{232}Th. At low energies, central collisions lead to complete fusion, whereas peripheral collisions proceed by deep-inelastic scattering.[9]) The division appears to be set by a critical radius, i.e.

$$R_c \simeq 1.0\ (A_1^{1/3} + A_2^{1/3}),$$

where the nuclei overlap at their half-density points.[10]) In this region, an additional reaction mechanism of fast fission may occur[11]) on a time and impact parameter scale intermediate between the other two mechanisms. At high energies we show the transparency discussed above, along with the peripheral participant-spectator process and, in more central collisions, the complete explosion. It would probably be unproductive at present to attempt to understand these reactions solely in terms of nucleon-nucleon collisions, although some day it will no doubt be possible to do so. The main sections of the diagram represent well established reaction processes; they are the corner stones of the final structure. Less clearly defined at present are the boundaries between the regions, but it is clear that intermediate energy collisions are ideally suited to map out the details of the transitions.

3. Transitional phenomena

There are already several intimations of transitional phenomena. At energies between 15 and 20 MeV/nucleon, new processes of incomplete fusion[12]) and incomplete deep-inelastic scattering[13]) have recently been discovered. Here only part of the projectile is captured by the target, and the other part escapes immediately. Fast fragments are produced, which in some sense could be regarded as the precursors of the more violent disruption of the nuclei observed at high energies, and which are represented schematically in Fig. 2. A useful framework for the discussion of the high energy behavior is the participant-spectator model,[14]) in which a source of intermediate rapidity, equal to one half the beam rapidity in the case of equal mass target and projectile, is formed from the overlapping portions of the nuclei. This source constitutes the high temperature participant zone. The remaining parts of projectile and target are the cold spectators.

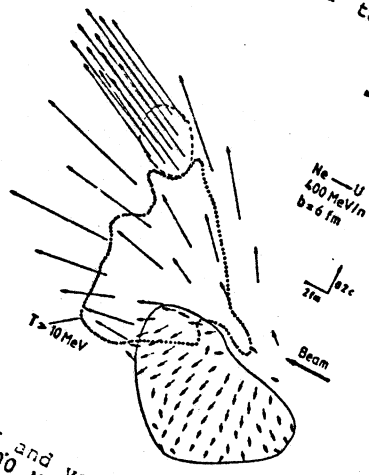

Temperature, density and velocity profiles for hydrodynamical ion of ^{20}Ne + U at 400 MeV/nucleon.

This simple idea is justified more formally by hydrodynamical[15] and cascade calculations.[16] An example is shown in Fig. 3 of the temperature density and velocity profiles for Ne on U in a peripheral collision at 400 MeV/nucleon.[15] This concept of a nuclear collision differs markedly from our low energy ideas. In the TDHF approach, for example, the interaction is mediated by the mean field,[17] rather than by two-body collisions in the participant zone. Also the low energy phenomena of deep-inelastic scattering allows the energy to be equilibrated over the entire nuclear system, rather than localized in the participant region.

We can identify some characteristic properties of spectators and participants. By observing light particle emission in the rest frame of the participant zone in a rapidity plot, the spectra can be fitted by the function $\sqrt{E}\exp(-E/T)$ to derive a value of T. This exercise has been undertaken for a variety of colliding systems at energies from 58 MeV/nucleon[18] up to 3.6 GeV/ nucleon.[1] The results are collected in Fig. 4, and plotted as a function of energy/nucleon above the barrier. The temperature increases smoothly, up to 3.6 GeV/nucleon where it is close to the value of 140 MeV. The behavior beyond this point is of interest, since in some theories this temperature is a limit, arising from the fact that energy is more easily used to create new elementary particles in the participant zone than to add energy to the existing particles.[19] In the special case of an exponential growth of particle states the temperature limits at the "boiling point of hadronic matter". The behavior expected from quark models of elementary particles is a topic of current interest.[20] For the present we infer from the uniform trend of the temperature with energy that a participant zone can be identified, at least down to energies of 58 MeV/nucleon. Recent work shows that the description may be valid down to an energy of 32 MeV/nucleon.[21]

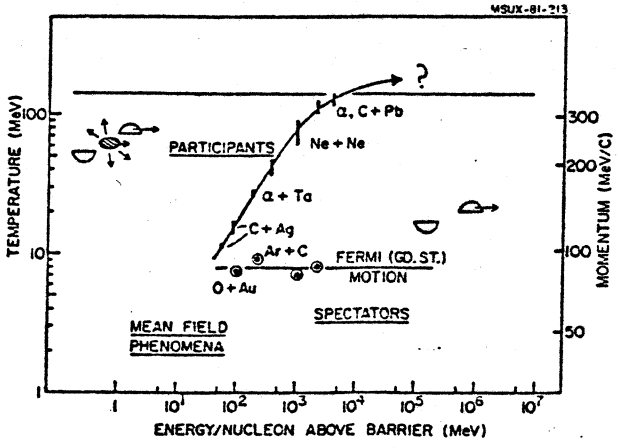

Fig. 4 Plot of momentum widths of spectator fragment distributions (right hand scale) and participant zone temperature (left hand scale) as a function of energy/nucleon.

A characteristic feature of the spectators is their momentum distribution, which provides a snapshot of the motion of the fragment

in the parent nucleus prior to the sudden abrasion.[22]) In the rest frame of the projectile (A) the fragments (F) have a distribution in momentum, $\exp(-p^2/2\sigma^2)$ where

$$\sigma^2 = \sigma_o^2 \frac{F(A-F)}{(A-1)} \quad \text{and} \quad \sigma_o^2 = \frac{1}{5} p_f^2$$

(i.e. in the case of F=1, we recover the value of σ^2 for a single abraded nucleon to be $\frac{1}{5}p_f^2$). Average values of σ_o have been deduced for many final fragments in reactions over a wide range of incident energies. These values are also plotted[1]) in Fig. 4 using the scale at the right and are seen to cluster around the value 80-90 MeV/c. Although this value is somewhat smaller than the expectation based on determinations of Fermi motion in electron scattering[23]) (viz. $p_f \simeq 240$ MeV/c, $\sigma_o = 107$ MeV/c) we take the uniform trend as an indication that the spectators, like the participants, can be isolated over a wide energy region from 90 MeV/nucleon to 2 GeV/ nucleon; again recent results are consistent with the above statistical fragmentation model at 32 MeV/nucleon.[21]) In the past some aspects of the scheme presented in Fig. 4 were carried down even to energies as low as 20 MeV/nucleon,[1]); more detailed studies show that the spectator process is not really developed at these energies.[24]) The low energy region is ascribed the label "mean field phenomena" in Fig. 4, to emphasise that here the energy is shared over the entire interacting system rather than divided between spectators and participants.

Turning to more central collisions, there are also indications for changes in the nature of the reaction mechanism between 20 and 80 MeV/nucleon. Studies have been made of the momentum transferred to the target nucleus through a measurement of the opening angle of the subsequent fission fragments.[25-27]) The lower half of Fig. 5 shows the distribution of fission fragments in coincidence with fast protons at forward angles for ^{16}O on U at 20 MeV/nucleon. The presence of two peaks in the distribution implies two dominant momentum transfers. The peak close to 173°, corresponding to the smaller transfer, i.e. to the more slowly moving fissioning system, is associated with peripheral processes, since it is the only peak observed in coincidence with projectile fragments such as Li and B which are known to be created in peripheral collisions. The large momentum transfer ($\theta_{AB} = 148°$) is then attributed to central collisions; the ratio of the two contributions is roughly in accord with the critical radius concept mentioned in the discussion of Fig. 2. Since the location of the peak for central collisions is consistent with a recoil momentum equal to the difference between the incident beam momentum and that carried off by the observed fast proton, in all likelihood the reaction is one of incomplete fusion; as indicated in Fig. 2, a fast proton escapes immediately and the remaining part of the projectile fuses with the target, imparting the remaining momentum. The top part of Fig. 5 shows that the behavior is apparently quite different at 86 MeV/nucleon.[1,28]) The central component does not appear to exist for fission fragments in coincidence with 0, 1 or 2 fast protons detected in a forward angle hodoscope. We infer that at these energies central collisions result in disruptions of the nuclei more drastic than the fission process. Possibly the complete explosion depicted in Fig. 2 is already taking place.

To emphasize further the significance of the region of 20 MeV/nucleon, Fig. 6 summarizes the results of several experiments of the above nature.[29]) In order to compare reactions induced by different projectiles ranging from protons to ^{20}Ne, the value of the momentum transfer per nucleon, $\langle p_{\perp} \rangle / A$, is plotted. A deviation from full momentum transfer leading to fission sets in at approximately 15

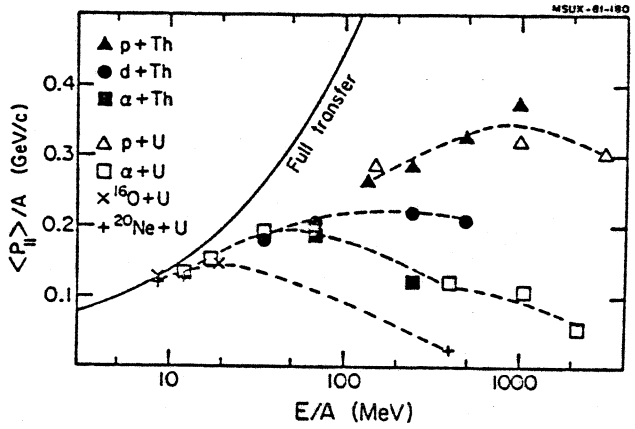

Fig. 6 The parallel momentum transferred per nucleon for different reactions as a function of energy/nucleon.

on Au and Al. At much higher energies of 250 to 1000 MeV/nucleon, multiplicities have also been determined[32] and are shown for ^{20}Ne or U. Here the multiplicities are commensurate with the number of particles expected in the participant zone. For the strict fireball

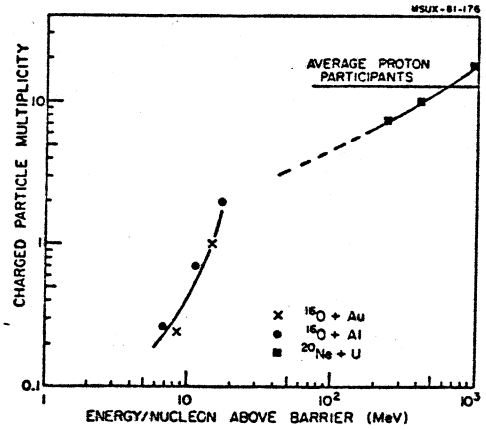

Fig. 7 Charged particle multiplicity as a function of incident energy/nucleon above the barrier.

geometry this number is 13 in the above case; in a more sophisticated firestreak treatment[33] the multiplicity is energy dependent, following the trend of the data[32]. Once again we see that the intermediate energy regime of 20 to 200 MeV/nucleon may establish the transition between characteristic low and high energy processes.

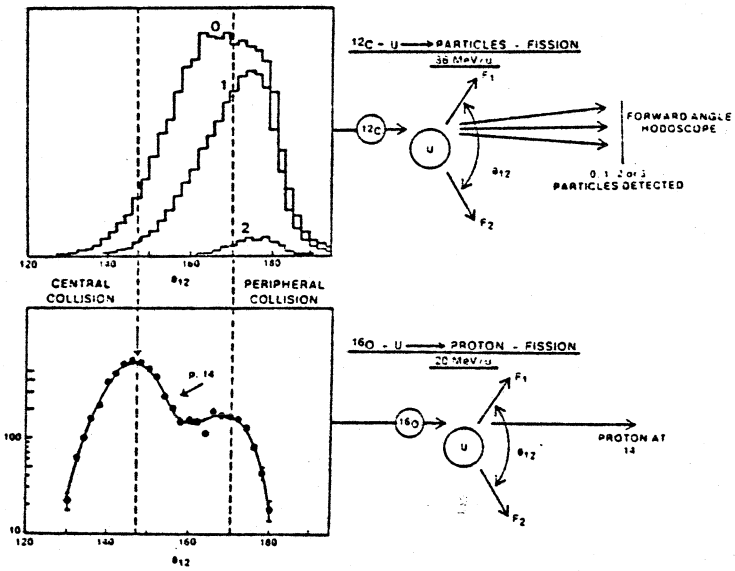

Fig. 5 Comparison of the distribution of opening angles of fission fragments in coincidence with forward going light particles for ^{12}C + U at 86 MeV/nucleon (top) and ^{16}O + U at 20 MeV/nucleon (bottom).

MeV/nucleon, and the reduction becomes quite drastic above 35 MeV/nucleon. As discussed above, the effect is most likely due to the onset of fast particle emission. The threshold at 15 MeV/nucleon can be understood by invoking the balance of nuclear, Coulomb and centrifugal forces to determine[12,30]) a critical angular momentum ℓ_c:

$$4\pi\gamma\frac{R_1R_2}{R_1+R_2} = \frac{Z_1Z_2e^2}{(R_1+R_2)^2} + \frac{\ell_c(\ell_c+1)\hbar^2}{\mu(R_1+R_2)^3}$$

One finds that by 20 MeV/nucleon the critical angular momentum for all fragments of the projectile is exceeded and it is natural therefore to expect an onset of fast light particle emission. In a broader context one might note that 15 MeV/nucleon is also close to the velocity of sound in nuclei, as determined from the compressibility constant K≈200 MeV of the giant monopole mode, $v/c = \sqrt{K/9m_o}$. Another important parameter is the mean Fermi velocity of a nucleon, equivalent to about 28 MeV/c. These two velocites determine characteristic relaxation times in the nucleus. All these criteria may conspire to enhance the role of the intermediate energy region as one of change in the nature of the reaction mechanisms.

Yet another aspect of change in the intermediate regime is illustrated[31]) in Fig. 7, by the increase of charged particle multiplicity (protons to alphas) as a function of incident energy; particles of intermediate rapidity are selected, excluding those from compound nuclear, equilbrated processes or from projectile excitation and decay. The multiplicity, defined as the ratio of integrated charged particle cross section divided by σ_R, the reaction cross section, increases rapidly between 5 and 15 MeV/nucleon[27]) for the systems ^{16}O

As a final example of transitional behavior we mention a theoretical calculation. Using perturbation theory it has been shown[34]) that the transition probability for a heavy-ion reaction leads to an expansion of the cross section in terms of y, the ratio between the duration of a nucleon-nucleon collision and the elapsed time between two successive interactions. The variation of y with energy is shown in Fig. 8, and demonstrates that there is a transition from Markovian to non-Markovian behavior between 20 and 200 MeV/ nucleon. The increase in y at high energies comes about from the reduction of Pauli blocking as the frequency of collisions becomes high. The observable consequences are most pronounced in the width of the final mass distribution of emitted fragments. The shortening of the mean free path and the reduction of Pauli blocking also diminish the importance of mean field phenomena, and set the stage for hydrodynamical approaches.

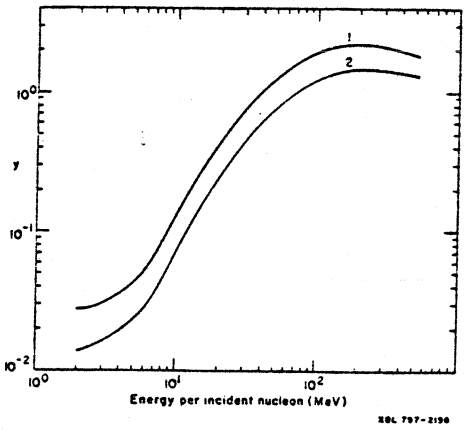

Fig. 8 The parameter y, the ratio of the two-nucleon collison time to the time between subsequent interactions, as a function of the incident energy/nucleon. The two curves correspond to different interaction potentials.

For the above discussion it is clear that intermediate energies are fertile territory for enriching our knowledge of nuclear collisions. In the remainder of this paper we discuss the current situation in peripheral collisions, dealing mainly with the production of heavy fragments in central collisions, which result predominantly in light fragment emission, and finally we discuss some exotic topics relevant to intermediate energy.

4. Peripheral reactions

Various experiments with electrons, mesons, protons and alpha particles have resulted in a consistent and detailed picture of nuclear charge and matter densities. However, we have very little knowledge of the variation in speed of a nucleon as it moves from the surface to the center of the nucleus. The spectator fragments produced in heavy-ion collisions may convey some information on this distribution.[35])

Suppose[22]) that A nucleons in the projectile are assembled with zero net three momentum, $\langle P_A \rangle = 0$. If F of these nucleons, chosen at random, are suddenly released as a single fragment, what would be the mean square momentum P_F? Each of the nucleons has a mean square momentum $\langle p^2 \rangle$ correlated by the constraint $\langle P_A \rangle = 0$, and

$$P_F^2 = \langle (\sum_{i=1}^{F} p_i)^2 \rangle = \frac{F(A-F)}{A-1} \langle p^2 \rangle ,$$

where $\langle p^2 \rangle = \frac{3}{5} p_f^2$, the mean square Fermi momentum. A measurement of each Caresian component of the momentum distribution yields a distribution in momentum, $\exp(-p^2/2\sigma^2)$, with

$$\sigma^2 = \frac{p_f^2}{5} \frac{F(A-F)}{(A-1)}$$

A good illustration from reactions of ^{40}Ar at 213 MeV/nucleon is shown in Fig. 9 by the Gaussian distribution of the momentum (actually energy is plotted) of ^{34}S fragments.[36]) The distribution peaks at an energy corresponding closely to the fragment, ^{34}S, traveling with the

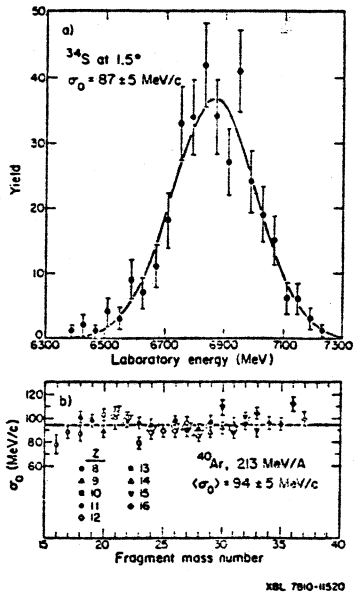

Fig. 9 The upper section shows the energy spectrum for ^{34}S fragments produced by ^{40}Ar on ^{12}C at 213 MeV/nucleon. The widths of the momentum distributions σ_o (see text) for all observed fragments are shown below.

incident beam velocity, as we expect for a projectile spectator fragment. The values of σ_o deduced from the Gaussian fit in momentum space to this fragment, as well as to all other observed fragments from Z=8 to 16, are shown at the bottom of the figure. The value of σ_o = 94 MeV/c corresponds to p_f = 210 MeV/c significantly lower than the value of 250 MeV/c for ^{40}Ar determined by electron scattering.[23])

It is not only at intermediate energies that values of σ_o below the mean Fermi values are found. Figure 10 gives the momentum distribution for ^{15}O fragments in the abrasion of a single nucleon from ^{16}O at 2.1 GeV/nucleon.[35] Note that this plot is made as a function of k_{11} (the parallel momentum component) on a log scale, so that, in terms of the earlier formula, the distribution would be just a straight line. In this case the uniform and local Fermi gas models fail to reproduce the results. We see that the shell model with harmonic oscillator wave functions is correct for momenta below the Fermi momentum, and that Hartree-Fock wave functions describe the data quite well over the full range. The point here is that this model gives a good description of the momentum distribution in the surface, where the nucleons are moving more slowly than in the interior. The electron samples the distribution over a large part of the nucleus.

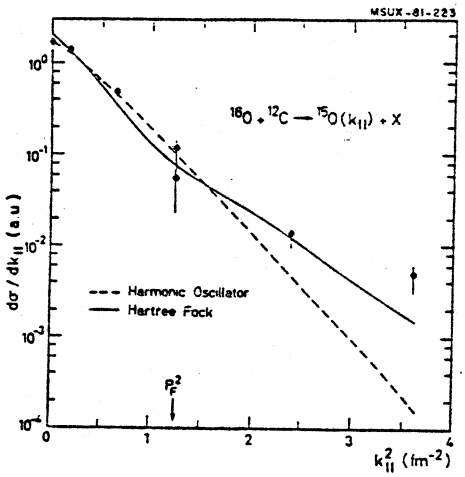

Fig. 10 Momentum distribution of ^{15}O fragments in the projectile frame as a function of k_{11}, compared with harmonic oscillator and Hartree-Fock shell-model predictions.

Nevertheless it seems unlikely that this explanation is responsible for the uniform reduction in σ_o for all the fragments observed in Fig. 9, since in the scheme of the spectator model these must span a wide range of impact parameters from the surface inwards. Another factor to be considered is the neglect in the single particle model of all correlations between particles other than simple kinematical ones. In particular, Pauli correlations should reduce the dispersion in the measurement of one-body operators.[37] An estimate for ^{40}Ar reduces the dispersion by 37%. There are also other more trivial processes which can reduce the momentum dispersion. In the production of fragments of one half the projectile mass, for example, there can be contributions from secondary decays of heavier primary products. Because of the parabolic dependence of the width on F(A-F) these primaries have a smaller intrinsic momentum dispersion, which is then reflected in the width of the subsequent decay fragments. However, this mechanism should increase the widths of fragments less than half

the mass, whereas all widths are narrower in Fig. 9. It is likely therefore that some effects of correlations are present in the data. In the case of fragmentation of uranium the reduction in the momentum dispersion by the Pauli effect is predicted to be a factor of two which, if observed, will be fairly dramatic.

The zero point motion has also been investigated through the isotope distributions, by the influence on the probability for abrading neutrons and protons.[38,39]) The giant dipole mode, for example, is an out-of-phase vibration of neutrons and protons perturbing the number of abraded nucleons as a function of impact parameter. In Fig. 11, theoretical distributions are compared with data

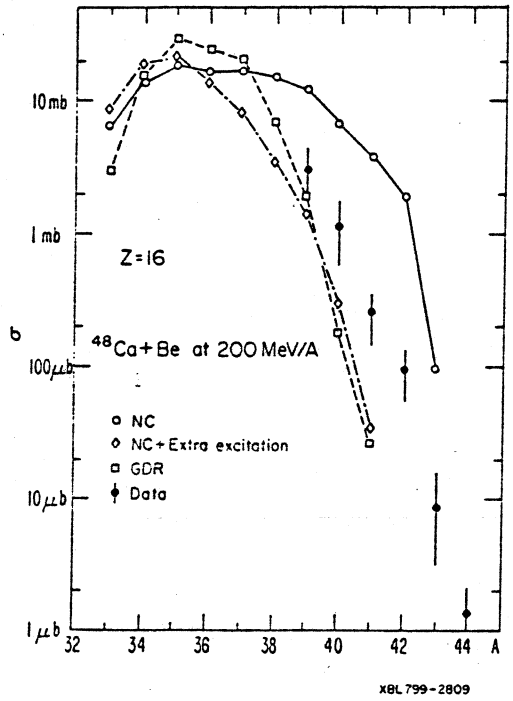

Fig. 11 Isotope distributions of sulfur fragments produced from ^{48}Ca + Be at 200 MeV/nucleon. The theoretical curves are explained in the text.

for sulfur isotopes in reactions of ^{48}Ca on Be at 200 MeV/nucleon.[40]) The distribution, including the effect of the dipole mode (GDR), is considerably narrower and closer to the data than the no-correlation, hypergeometric model in which protons and neutrons can be selected independently with the appropriate combinatorials. In these calculations the cascade de-excitation of the primaries is calculated by taking the initial exictation energy as the difference in surface energies of the abraded and the normal spherical shapes of the

fragments. As in the case of the momentum distributions, however, the effect of the correlations can be simulated by artificially injecting additional excitation energy into the primaries (the case of NC + extra excitation). Before this interesting and unique feature of energetic, heavy-ion collisions can be definitively pursued, a better model for the primary excitation is needed. This may be possible with cascade or Glauber model calculations for the primary stage.[41] The results of this approach, applied to isobaric distributions in ^{40}Ar reactions at 213 MeV/nucleon leading to a few representative A values, are shown in Fig. 12. It is found that although the distributions are certainly dominated by the level density of the final fragments at their lowest particle threshold, some properties of the fragmenting system enter via a memory factor. Comparisions of fragment distributions from nuclei with very different neutron excess like ^{40}Ca and ^{48}Ca could indicate the sensitivity remaining to the memory of the ground state correlations.

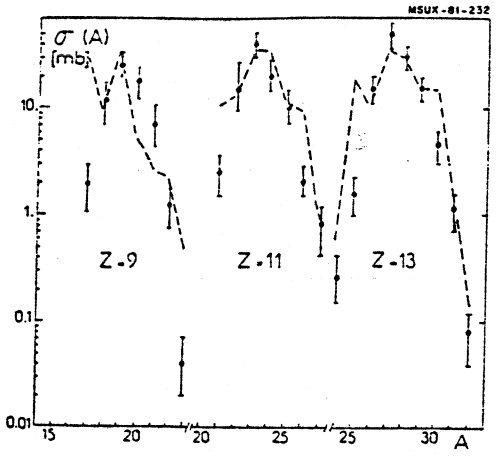

Fig. 12 Projectile fragmentation in the reaction ^{40}Ar + ^{12}C at 213 MeV/nucleon, compared with a theoretical calculation discussed in the text.

We turn now from these unusual features of the parallel momentum distribution to effects in the perpendicular component. According to the fragmentation model outlined in this section, the widths of all three Cartesian components should be equal, and such equality is established within 10% at relativistic energies.[42] The behavior appears to be different at intermediate energies of 100 MeV/nucleon, where the perpendicular component is substantially larger.[43] These widths, for reactions of ^{16}O on Al and Au at 117.5 and 92.5 MeV/nucleon, appear in Fig. 13. In all cases the values of σ_1 are larger than

$$\sigma_o^2 \frac{F(A-F)}{(A-1)} ,$$

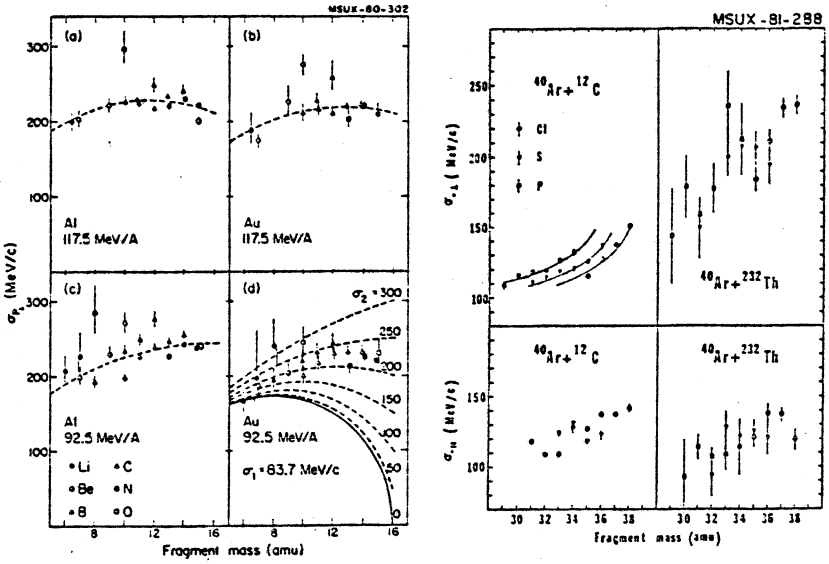

Fig. 13(left) The values of σ_1 for isotopes in (a) ^{16}O + Al at 117.5 MeV/u, (b) ^{16}O + Au at 117.5 MeV/u (c) ^{16}O + Al, at 92.5 MeV/u, (d) ^{16}O + Au at 92.5 MeV/u. The theoretical curves are discussed in the text; (right) $\sigma_\perp$ and $\sigma_{||}$ values for reactions of ^{40}Ar + ^{48}C and ^{40}Ar + Th at approximately 100 MeV/nucleon.

the equation we have used for $\sigma_{||}$ and which is shown by the solid curve, labelled σ_2=0, in Fig. 13(d). Greater sideways momentum is imparted to the fragmenting system. If we denote this momentum, whatever its origin, by $\langle P_A \rangle$, no longer equal to zero, with

$$\sigma_2^2 = \frac{1}{2} \langle P_A^2 \rangle,$$

then it can be shown that

$$\sigma_\perp^2 = \frac{F(A-F)}{(A-1)} \sigma_1^2 + \frac{F(F-1)}{A(A-1)} \sigma_2^2$$

and the effect of varying σ_2 is shown in the figure. The expected values of σ_2 have also been calculated from the classical deflection function of the projectile in the Coulomb and nuclear potentials, fixing the applicable range of impact parameters from the ratio of the observed fragmentation cross section to the reaction cross section. The required values of σ_2 ranging from 170-200 MeV/c are reproduced with a Saxon-Woods potential 70 MeV deep. If this approach stands the test of time, we may have at our disposal a means of probing the nuclear potential to much greater depths than hitherto possible in elastic scattering and transfer reactions.[43] The range of impact parameters encompassed by the above experiments is shown in Fig. 14 by the shaded areas. We must emphasize, however, that there is a systematic dependence of σ_2 on isotope (see Fig. 13) which is not at all accounted for by this model. These trends are even more pronounced

in the case of ^{40}Ar fragmentation at 118 MeV/nucleon.[44] In Fig. 13(right hand side) the variation in the parallel and perpendicular widths for ^{40}Ar on Th and C are displayed as σ_o^{11} and $\sigma_o^{\perp}$, defined by

$$\sigma^2 = \sigma_o^2 \frac{F(A-F)}{(A-1)} \quad .$$

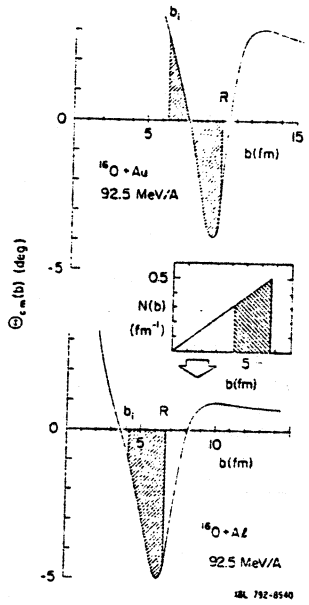

Fig. 14 Deflection functions for ^{16}O + Al, ^{16}O + Au at 92.5 MeV/u. Insert shows range of impact parameters for fragmentation.

In this case not only $\sigma_\perp$ but also σ_{11} deviates considerably from the value ≈90 MeV/c typical of higher energies. Increases in σ_{11} have also reported for ^{12}C reactions at 86 MeV/nucleon,[45] but we note that for the ^{16}O reactions shown[43] in Fig. 13(left), the value was normal (denoted there as σ_1 = 83.7, which is the same as σ_o in the above notation).

In addition to this classical deflection, the trajectory may be influenced by quantal dispersion and by energy dissipation.[46] Both effects are well known in low energy deeply-inelastic scattering, where the transport equation can be reduced to equations for the mean trajectory and its spread. Applying these methods to the ^{16}O + Al data at 92.5 MeV/nucleon, the scattering angle θ, the final kinetic energy, E_f, and dispersion Δ_θ in Fig. 15 are derived; the relevant impact parameter region from Fig. 14 is also indicated. While the angular width and the energy loss are of the correct magnitude, the parameters necessary for this agreement differ from the low energy deeply-inelastic case. In particular it is necessary to increase the value of the parameter characterizing the energy dependence of the nuclear transition matrix element. One interpretation is that only

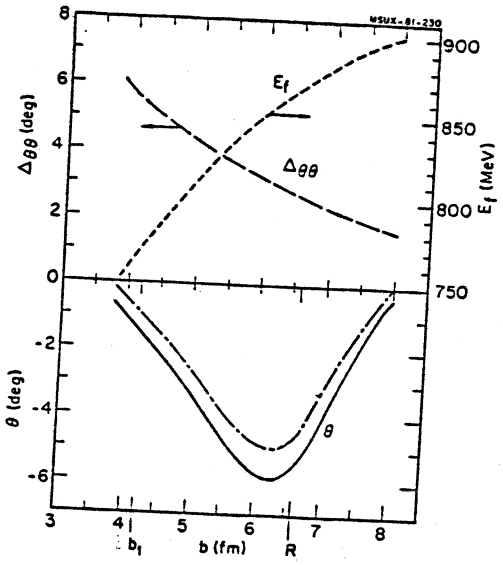

Fig. 15 Scattering angle θ, final kinetic energy E_f and angular width Δ_θ as functions of impact parameter b for reactions of ^{16}O + Al at 92.5 MeV/nucleon.

local excitations are important, since the reaction time at 100 MeV/nucleon is comparable to the time it takes the perturbed nucleus to attain global equilibrium. Here we have an indication, albeit an indirect and circuitous one, that localized excitations, or hot zones, may be formed in intermediate energy collisions. We shall discuss such zones in detail in the next section. They are also a feature of hydrodynamical models (see Fig. 3), and it is conceivalbe that the large transverse momenta we have discussed in this section reflect the compressional bounce-off effects of hydrodynamics.[47]) There could also be a contribution from scattering of participant nucleons into the spectator fragments.

5. Central collisions

We have already indicated in Fig. 3 that a prominent feature of collisions at intermediate and high energies is the fast spray of high multiplicity light particles. A graphic illustration[3]) is the streamer chamber photograph of ^{40}Ar in collision with BaI_2 at 60 MeV/nucleon in Fig. 16. This behaviour seems to be typical of several theoretical approaches, two of which are compared in Fig. 17. On the left[48]) are the density contours of a TDHF calculation for ^{12}C + Au at 30 MeV/nucleon for peripheral (b=6fm) and central collisions (b=1 fm). The outermost contour line has $\rho = 0.14 \times 2^{-NC+1}$ nucleons/fm^3 and successive inner contours have densities lower by a factor of 2. In the central collision a high velocity jet of dilute matter escapes, equivalent to about 8 nucleons. In the peripheral collision the main part of the projectile orbits to the opposite side of the nucleus, while some fast particles escape, reminiscent of the incomplete fusion mechanism. In part (b) collisions between particles are incorporated

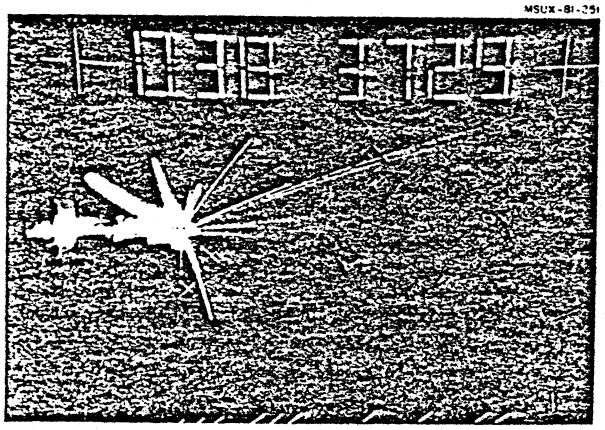

Fig. 16 Central collision of 60 MeV/u ^{40}Ar with BaI_2 in a streamer chamber.

into the TDHF method which then describes the passage of ^{16}O through ^{40}Ca at a higher energy of 250 MeV/nucleon.[49] There occurs a rapid increase in density leading to a positive increase of the mean field potential in the overlapping region. The resultant "volcano effect" causes some of the nucleons to become unbound, lowering the depth of the mean field potential and ending in the complete disintegration of the ^{16}O nucleus into vortex rings of dilute Fermi gas. As we have seen in Fig. 3, these phenomena are also characteristic of hydrodynamical models. Presumably the inclusion of two-body collisions makes the TDHF calculation contain some features of the hydrodynamical approach, a marriage which must surely be consummated at intermediate energies.

From the above discussion, it is obvious that central collisions of nuclei, even at intermediate energies, are very complicated. Since it is very likely necessary to measure the properties of all emergent particles, to obtain meaningful information from only one seems like a hopeless undertaking. Complete event reconstruction for intermediate energies is at an embryonic stage with the streamer chamber.[3] Meanwhile the inclusive measurements do give us intimations of interesting phenomena. The inclusive spectrum of protons from ^{12}C + Au at 86 MeV/nucleon in Fig. 18, for example, suggests evaporation from a source moving in the laboratory frame.[18] In the rest frame of this source the spectra at all angles would have the same slope, reflecting the temperature. Taking the rest frame spectrum as $\sqrt{E}\exp(-E/T)$, the transformation to the laboratory yields, non-relativistically,[25-27,50]

$$\frac{d^2\sigma}{d\Omega dE} \propto N_o\,(E-E_c)^{\frac{1}{2}} \exp - \left(\frac{E-E_c+E_1-2E^{\frac{1}{2}}E_1^{\frac{1}{2}}\cos\theta}{T}\right)$$

where E_c is the kinetic energy gained by Coulomb repulsion, $E_1 = \frac{1}{2}mv$ is the kinetic energy of the particle moving with the source velocity, v, and N_o is an overall constant. The relativistically invariant form is,

$$\frac{Ed^2\sigma}{p^2dpd\Omega} \propto N_o(E-\beta p\cos\theta)\ \exp\left\{-\gamma\frac{(E-p\beta\cos\theta)}{T}\right\}$$

with $\beta=v/c$, $E=(p^2+m^2)^{\frac{1}{2}}$, $\gamma=(1-\beta^2)^{-\frac{1}{2}}$ (Here the correction for Coulomb repulsion is not included). These formulae give a remarkably good

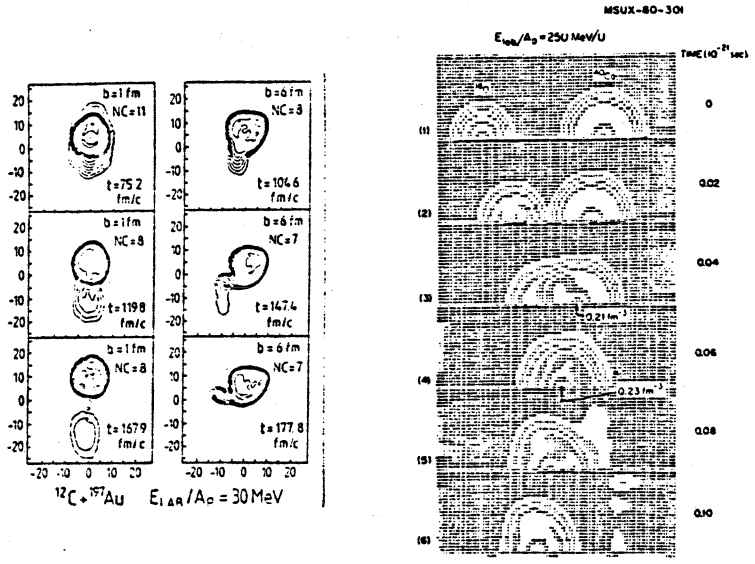

Fig. 17 TDHF calculations for ^{12}C + ^{197}Au at 30 MeV/nucleon (left) showing density contours for central (b=1 fm) and peripheral (b=6 fm) collisions; on the right are TDHF calculations, with collision terms, of the break-up of ^{16}O on ^{40}Ca at 250 MeV/nucleon.

description of the high energy tails of proton spectra in heavy-ion reactions ranging over an energy of a few MeV/nucleon to 1 GeV/nucleon. The fitting is usually made at angles larger than 45°, thereby emphasizing central, high P_L events and minimizing the contribution of projectile excitation, decay and fragmentation. In some cases a more stringent requirement is imposed; for example at low energies, as we discussed for Fig. 5, a central collision fission trigger can be required;[25-27] at high energies a high multiplicity trigger creates a bias towards central events.[51])

The systematic dependence of the extracted source temperature on the incident energy per nucleon is shown in Fig. 19. In all cases the source velocity is close to half the beam velocity. Referring back to Fig. 3, an obvious candidate for this source, at least at high energies, is the participant zone, although it moves with half beam velocity only in the special case of equal mass target and projectile. In general the strict fireball geometry gives[52]) a source velocity,

$$\beta = \frac{P_L}{E_L} = \frac{N_p\ t_1(t_1+2m)}{(N_p+N_T)m+N_p t_i}$$

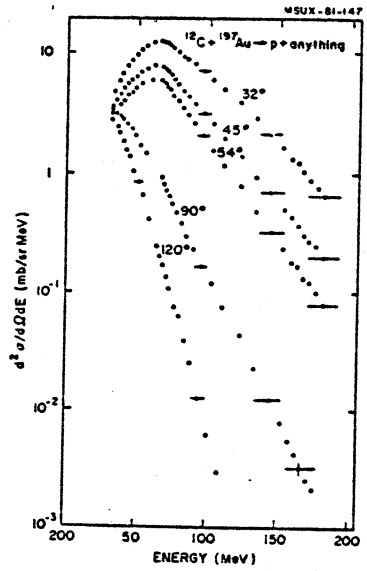

Fig. 18 Cross section, $d^2\sigma/d\Omega dE$ for protons emitted in $^{12}C + ^{197}Au$ at 86 MeV/nucleon.

where P_L, E_L are the momentum and total energy in the laboratory frame, t_i is the incident energy in MeV/nucleon, m is the nuclear mass, and N_P, N_T are the number of participant nucleons from projectile and target. The systematics derived for the reactions in Fig. 19 imply that N_P is always roughly equal to N_T. We should note that the participant zone is discussed with much more sophistication in the elaborate theoretical models of the firestreak,[33,53] two-fireball,[54] cascade[55] and hydrodynamics.[15] The simple parameterization presented here is intended to capture the spirit of these models and to highlight the uniform trends.

If we assume that the source is composed of equal numbers of contributing nucleons from projectile and target, then the excitation energy, E^*, is related to the incident energy per nucleon above the barrier,[50] $(E-V_C)/A$ by

$$E^* = \left(m_o^2 + \frac{1}{2} m_o \, (E-V_C)/A \right)^{\frac{1}{2}} - m_o$$

At low energies where $(E-V_C)/A \ll m_o$, then

$$E^* = \frac{1}{4} \left(\frac{E-V_C}{A} \right)$$

which we equate to $T^2/8$, the low temperature Fermi gas equation of state. In general $E^* = \langle E(T) \rangle - \langle E(T=0) \rangle$ with $\langle E(T) \rangle$ computed from the complete Fermi distribution function, and $\langle E(T=0) \rangle = 3/5\epsilon_f$. The relation between T and $(E-V_C)/A$ at all energies is shown in Fig. 19

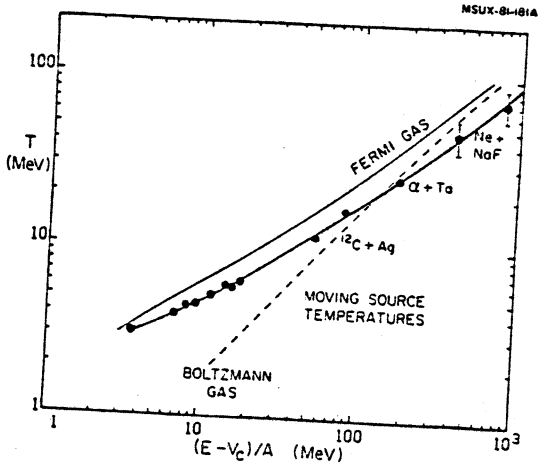

Fig. 19 Temperature parameter for protons emitted from a source with rapidity of about one half the beam value in various reactions.

by the solid line. For comparison the equivalent line for a Boltzmann gas is also illustrated; of course at high temperatures the two formulations approach one another. The measured temperatures follow the trend of the Fermi gas prediction, but are always slightly lower. Noteworthy here is the consistency obtained between α [56] and heavy-ion induced reactions, which is also true at much higher energies[1] of 3.6 GeV/nucleon (see Fig. 4). The stability of description is indicative of common underlying reaction mechanisms. It is not possible, however, to infer for certain that the explanation is one of thermal equilibrium in a localized zone consisting of a Fermi gas. For example, the half-beam velocity also suggests the importance of a nucleon-nucleon frame of reference. It is important to establish the contribution of single and multiple nucleon-nucleon collisons over the whole energy domain, (see refs. 57-61 and references therein). At high energies, above 800 MeV/nucleon, it is already known that some 30% of collisions of Ne on U do lead to complete thermal equilibrium, [59] but the equivalent studies are not yet made at low energies. [62]

Taking the results at face value, the existence of a localized, hot zone is implied. Its creation poses something of a problem, at least at low and intermediate energies. One condition is a short mean free path, apparently in contradiction both to the experimental data on low energy nucleon scattering as well as to the success of mean field theories based on the long mean free path assumption. On the other hand, the validity of hydrodynamics relies on a short mean free path; it is therefore quite important to establish the correct relevant mean free path at all energies and temperatures. A resolution of the conflicting requirements may be contained [63] in Fig. 20. As the temperature increases the effect of the Pauli exclusion principle diminishes, so that two-body collisions dominate

over the mean field collisions with the wall. Thus, even at low energies, as the temperature approaches 10 MeV, the mean free path tends to the high energy limit of $1/\rho\sigma \approx 2$ fm. This reduction of the mean free path within the hot zone could provide a self containing mechanism for the local excitation. The mean free path shown for zero temperature is commensurate with experimental values deduced [57] from the depth of the imaginary potential, viz.,

$$= \frac{1}{W} \sqrt{\frac{(\hbar c)^2 E}{2mc^2}}$$

However, recent experimental and theoretical results indicate that the mean free path at T=0 may be longer than hitherto believed.[64]) Other discussions of the relevant mean free path for nucleus-nucleus collisions are given in ref. 65.

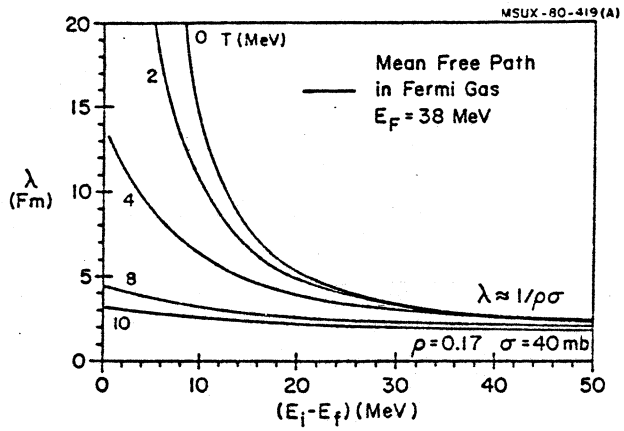

Fig. 20 Theoretical predictions of the nucleon mean free path as a function of energy above the Fermi energy for different nuclear temperatures.

Quite elaborate hot-spot theories have been developed[66-68]) in which the classical heat transport equation,

$$\frac{\partial}{\partial t} T(r,t) = 1/\rho c_p \, \nabla\cdot(K\nabla T(r,t))$$

is solved for the temperature field T, where ρ is the nuclear density, K the thermal conductivity and c_p is the specific heat of nuclear matter. The quantity K, like the mean free path, is itself temperature dependent. The theory predicts asymmetries in the emission pattern of the light particles from the zone. Although there is some evidence for this behaviour already at low energies of 5 MeV/nucleon,[69]) perhaps the most convincing experiment[70]) and theoretical analysis come from the realm of high energy hadronic reactions.[70]) Here it is conjectured that high energy pions may be evaporated from a hadron after the localized excitation has started to propagate but before the energy is spread evenly over the hadron. The effect has been searched for in the reaction $K^- + p \to K^- p \pi^+ \pi^-$ at 14 GeV/c. According to the diagram in

Fig. 21, more high energy pions should be radiated from the hot spot formed at the south pole than from the north pole. The distribution as a function of cosθ appears to contain this effect, whereas the φ distribution has no asymmetry. Experiments of this type are being used to determine the relaxation time constants of hadronic [68]) and nuclear matter,[71,73]) although few results are available in cases of heavy-ion collisions.[74]) In fact it seems that most coincidence measurements between light and heavy fragments which are necessary to establish the asymmetry, can be explained using other mechanisms, such as projectile fragmentation or delayed fragmentation,[75]) and orbiting

MSUX-81-148

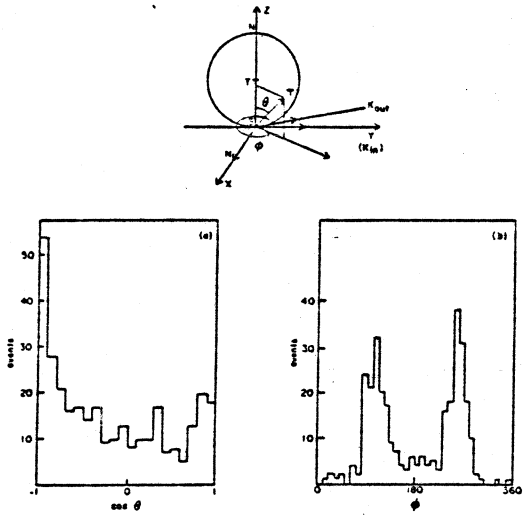

Fig. 21 Schematic representation of pion production from hadronic hot spot for the reaction $K^-p \to K^-p\pi^+\pi^-$ at 14 GeV/c. The distribution of pions in polar angles (cos θ) and in azimuth (φ) are shown in (a) and (b).

of deep-inelastic fragments.[76]) However, our understanding of the coincidence experiments at present is far from complete.[77,78] Experiments on backward production of light particles also show many similarities at low and at very high energies. Thus the 180° emission of protons in reactions of 90 MeV protons on various targets[79]) and in reactions induced by protons between 0.6 and 400 GeV[80]) have been analyzed with hot-spot models. There are also more mundane interpretations based on fragmentation models[81]) and on the exponentially falling virtual momentum spectrum of nucleons in nuclei.[82]) Perhaps these superficially different interpretations have some common features.

Further evidence for a hot zone comes from attempts to measure the size of the participant region. It is instructive first to use geometrical considerations.[14]) The average number of participants which come from the beam nucleus $\langle Z_B^P \rangle$ can be calculated as follows. If a proton in the projectile hits the target it becomes a participant:

$$\langle Z_B^P \rangle = Z_B \pi r_o^2 A_T^{2/3} / \sigma_R$$

where σ_R is the reaction cross section. Similarly

$$\langle Z_T^P \rangle = Z_T \pi r_o^2 A_B^{2/3} / \sigma_R .$$

Thus the total charge multiplicity of the participants is

$$\frac{Z_T A_B^{2/3} + Z_B A_T^{2/3}}{(A_B^{1/3} + A_T^{1/3})^2}$$

For the case ^{20}Ne + U, the value is 13, which is shown on the charged particle multiplicity plot in Fig. 3. The observed multiplicities at high energies are of this order; in the more sophisticated treatment of the nuclear firestreak model,[33]) the multiplicity becomes a function of the incident energy, following the trend of the experimental data.[32]) The number of participant neutrons is comparable but slightly higher, and the total number of participant particles is ≈30. At low energies of 20 MeV/nucleon, the high energy tails of the proton spectra have been analysed with a hot-zone model.[72,73]) The volume of the zone was deduced to be about 160 fm^3, corresponding to approximately 30 particles at normal density. Recalling the trends in Fig. 3, one might speculate that the multiplicity will approach the participant limit at an energy where the system can be completely disassembled. Although the correspondences at this stage may be coincidental, it is interesting to note that similar source sizes arise in the analysis of composite particle production, as discussed below.

There are two current approaches to the production of light composite particles in heavy-ion collisions. The coalescence model[83]) determines the probability for condensation of nucleons, which takes place if they lie within a coalescence radius p_o. The probability of finding a nucleon in a sphere of radius p_o centered at p is:

$$P \propto (\tfrac{4}{3}\pi p_o^3) \frac{d^2\sigma_1(p)}{p^2 dp d\Omega}$$

To obtain thecross section, we taken the probability of finding A-1 nucleons in the sphere p_o, multiplied by 1/A times the cross section for the emission of one additional particle. The final expression takes the form,

$$\frac{d^2\sigma_A}{p^2 dp d\Omega} \propto \frac{1}{A!} \left(\frac{4\pi p_o^3}{3\sigma_o}\gamma\right)^{A-1} \left[\frac{d^2\sigma_1}{p^2 dp d\Omega}\right]^A$$

where σ_o is the reaction cross section and γ is the relativistic correction factor. Once the cross section for single nucleon emission is known, the cross section for composite fragments is determined with only one additional parameter, p_o.

This power law dependence is, however, also expected in a thermodynamic model.[84]) Then the cross section for fragment emission is given by exp (-E/T) which can be written,

$$\exp\left[\left(\frac{-E/A}{T}\right)\right]^A$$

i.e. the single nucleon cross section raised to power A at the same MeV/nucleon. In spite of this equivalence, the physical content of the models is superficially different; actually in a more sophisticated treatment,[85]) they can be shown to be more closely related.

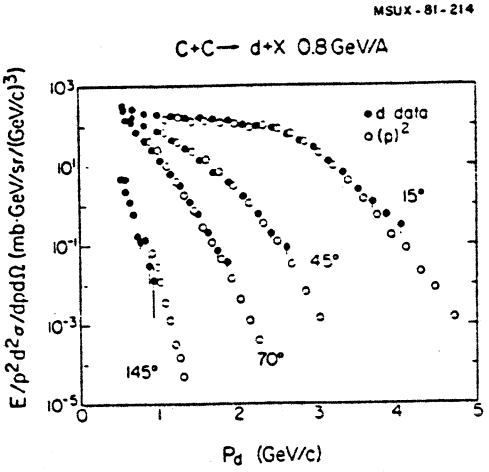

Fig. 22 Comparison of deuteron momentum spectra in the reaction, C + C at 800 MeV/nucleon, with the coalescence model.

The coalescence radius is an intrinsic property of the emitted particle and consequently should be independent of energy and mass of the colliding system. The equivalent constant of the thermodynamic model is related to the volume in which thermodynamic and chemical equilibrium is established. As such it is a property of the emitting region and will depend on the size of the nuclei forming it.[86]) Again, in a more thorough analysis[87]) the two effects must be folded together, i.e. there is a dependence on initial and final state interactions. Apart from numerical constants the parameters of the two models are related by

$$V \propto h^3/p_o^3$$

The power law dependence is followed rather closely at relativistic energies,[51,83]) as illustrated in Fig. 22 by the reaction $^{12}C + {}^{12}C \rightarrow d$ at 800 MeV/nucleon with a coalescence radius of about 213 MeV/c. Expressing the thermodynamic volume in terms of the radius of an equivalent sphere, values of R equal to 3.7 fm are typical. The prescription works over a wide variation of incident energy and colliding nuclei, including α particles in the initial channel, and even complex fragments like ^{6}Li in the final channel.[88])

The interesting physics comes from the trends of the parameters as a function of energy or mass. In Fig. 23 we show how the radius R (as defined above) depends on

$$(A_P^{1/3} + A_T^{1/3})$$

for many different colliding systems at a variety of energies. The vertical bars represent the range of values derived for different emerging particles, typically protons to ^{3}He. Results are included for α-particle induced reactions[38]) at 25 MeV/nucleon, for the ^{16}O

induced reactions[26,27]) at 20 MeV/nucleon which we have frequently discussed in this paper, and for results at relativistic bombarding energies of 400 - 2100 MeV/nucleon for many systems.[83]) There is a tendency for the radius to increase with

$$(A_p^{1/3} + A_T^{1/3}) ,$$

favoring the thermodynamic interpretation. We must note that other results for light-particle induced reactions, analyzed with a more microscopic model,[89]) are less supportive of this interpretation. From Fig. 23, however, we conclude that if the emission of complex fragments originates from chemical equilibrium in a localized source, then the radius is typically 3.5 fm; once again it is associated with about 30 particles.

Finally, in the determination of source sizes, we mention the more direct measurement of the space-time geometry by means of two-particle intensity interferometry.[90,91]) Results from experiments on detected pions are included in Fig. 23 and are consistent with the source radii determined from the emission of composite particles. It is less clear, however, that results with two-proton interferometry present a compatible picture of the size of the participant region.[92]) The method of interferometry will no doubt be applied soon over a wide

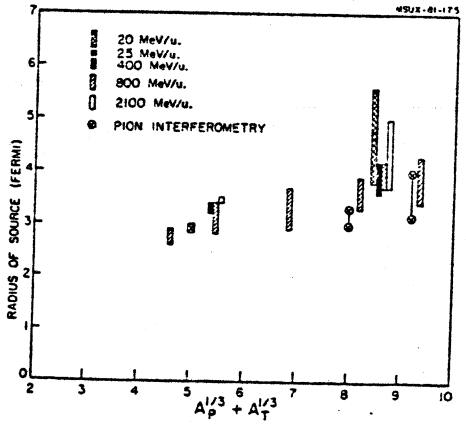

Fig. 23 Variation of effective source size in heavy-ion collisons as a function of $(A_p^{1/3} + A_T^{1/3})$ deduced from composite light particle production. Two results from pion interferometry are also shown.

energy range to determine source sizes. In addition to this application, it can also yield information on the degree of coherence or chaoticity in the source, and thereby on possible exotic conditions.[93]) Some of the exotic conditions pertaining to intermediate energy collisions are discussed in the last section of this paper.

6. Exotic topics

At high enough temperatures the localized, hot region will disintegrate or explode.[94] A minimum requirement is that the excitation energy per nucleon in the interacting volume of nucleons, composed of a_1 nucleons from the projectile and a_2 from the target, viz.,

$$E^* = E_{LAB} \frac{a_1 a_2}{(a_1+a_2)^2}$$

exceed 8 MeV, the average binding energy per nucleon.[74] If equal numbers of nucleons from projectile and target participant, $a_1 = a_2$ and $E_{LAB} = 32$ MeV/nucleon. The results of a more refined calculation,[94] with proper treatment of surface and volume effects, are shown in Fig. 24. The volume energy per particle as a function of compression $\eta = \rho/\rho_o$ at different temperatures is plotted, and is close to zero for T = 18 with $\eta = 1.3$. According to the systematics of Fig. 12, the required energy/nucleon is then ≈50 MeV/nucleon, when a high multiplicity of nucleons should be emitted from the zone. It is

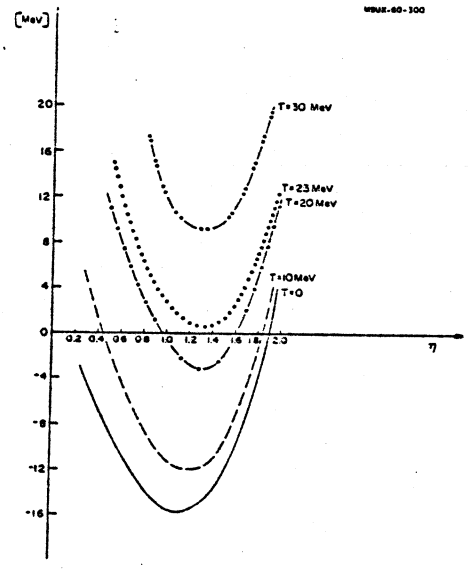

Fig. 24 The volume energy of nuclear matter per particle as a function of compression η at different temperatures T.

tempting to attribute the onset of this effect to the behaviour exhibited in Fig. 7, but more detailed studies are necessary over the important energy region from 20-100 MeV/nucleon. This type of study could yield results pertinent to the determination of the equation of state.[94] As we mentioned earlier, the disintegration of nuclear systems has also been investigated in the TDHF method,[49,95] in which the overlapping region of the two nuclei produces a rapid increase in

the density and an associated increase in the mean field potential. The resultant "volcano effect" makes the nucleons become unbound. Beyond the explosion temperature, there should be relatively few surviving composite particles.[96] Changes in the survival probability should be explored over the region in which the localized source appears to have been isolated (See Fig. 19). We already know that at high energies of 800 MeV/nucleon, the number of alpha particles[32,51] and heavier composites[97] is extremely small compared to protons. At energies below 20 MeV/nucleon, however, the number of alpha particles is still substantial,[27] of the order one half the proton multiplicity. The ratio must therefore switch over at intermediate energies; the rate at which this change occurs could tell us about the properties of nuclear matter at fairly high temperature and non-normal density.

A complete description of the disassembly stage of the hot transient system must incorporate the space-time development of the excitation energy distribution, which is beyond the scope of present theories. A start on this general problem has been made with a statistical model,[98] first applied to the problem of multiparticle production in high energy proton-proton collisions a long time ago.[99] In the primary explosion stage the system quickly fragments into nucleons and composite nuclei according to the available phase space. In Fig. 25(left) the variation of the overall fragment distribution with temperature is displayed. The parameter χ is a measure of the volume of the system and is of order unity in the case of normal density nuclear matter. Points corresponding to the same value of energy per nucleon are joined by the light curves. The horizontal dashed line for $\chi = \infty$ formally recovers the case of a classical gas of free nucleons where $T = \frac{2}{3}E$. For high temperatures most fragments appear as single nucleons and $A \to 1$. As a general consequence of composite fragment production, the temperature is higher than expected for a free nucleon gas, in agreement with results for the emission of heavy nuclei from a moving source in collisions with Ne and Argon beams[97,109] at 500 and 100 MeV/ nucleon. In Ne + U at 400 MeV/nucleon,[52] boron fragments of mid-rapidity were emitted from a source at a temperature of 27 MeV compared to a value of 13.5 MeV for a gas of free nucleons.

The neutron-proton ratio has also been calculated as a function of the temperature and of the volume parameter χ (see Fig. 25(right)). The measured ratio, n/p, from the participant zone for Ne + U at 350 MeV/nucleon[101] (actually the experiments for n and p were performed at slightly different energies) is plotted[102] in Fig. 26(b). At the low energy end of the spectrum the ratio is about 3, which is quite consistent with the results in Fig. 25(b). The relatively abundant composite fragments carry off roughly equal numbers of neutrons and protons, and hence act as an amplifier of the ratio of free neutrons to protons in a system of initial neutron excess.[98] (The dashed line is the fireball prediction ignoring composite formation.) From Fig. 26(a) we see that this effect may already present for ^{16}O on U at 20 MeV/nucleon; at the low energy end of the spectrum the neutrons (shaded) are approximately three times more abundant than protons.[103] The reason for the different slopes of the spectra remains a mystery however, as indeed it does in the high energy case. This discussion reinforces once again the unity of phenomena in nuclear collisions over a very wide energy region.

So far we have discussed exotic phenomena of the second kind. Those of the first kind concern possible new phases of nuclear matter, the conditions for which may only be attainable in heavy-ion collisions--if we discount remote areas of the Universe such as neutron stars. The attainable ranges of temperature and density, according to

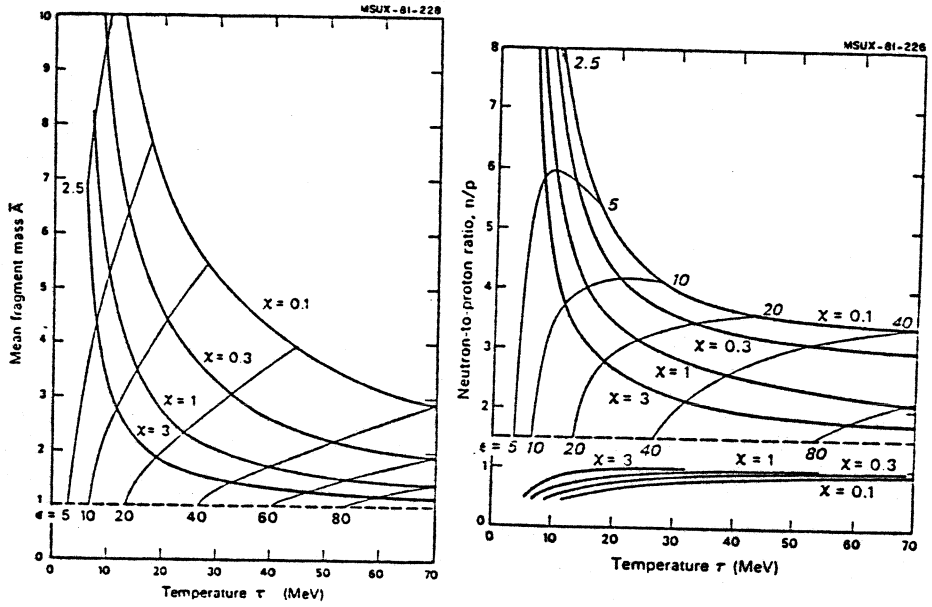

Fig. 25 (left) The average fragment mass number A as a function of the temperature T, for various values of the volume parameter χ. Points corresponding to the same value of the energy per nucleon ε are joined by the light curves; (right) the number of neutrons relative to protons as a function of temperature for isosymmetric systems (I=0, bottom) and typical neutron excess systems (I=0.2, top).

cascade calculations,[104]) are given in Fig. 27 together with a rough theoretical estimate of the boundaries for new phases of nuclear and hadronic matter.[105]) Two trajectories are illustrated, for collisions at 3.6 and 1.7 GeV/nucleon. It turns out that the lower energy achieves the higher density, the lower temperature for the longest period of time. The intermediate energy regime up to 200 MeV/nucleon may, therefore, turn out to be the best suited for reaching states related to pion condensation.

The problem is to find the experimental signatures of such a phase transition. One proposal[105]) is to search for a break in the slope of the invariant pion production cross section at $\theta_{cm} = 90°$ and $E_{cm} \approx 200$ MeV, since it can be shown that the coherent pions, originating from an ordered phase, peak at $k_{\parallel} = 0$ and $k_{\perp} \approx 2m_{\pi}$. The chaotic pions, on the other hand, are peaked at $k_{\parallel} = k_{\perp} \approx 0$ and fall off exponentially with $k_{\perp}$. At sufficiently low energies the chaotic component falls off so rapidly that the yield at $k_{\perp} \approx 2m_{\pi}$ could drop by 10^3 relative to the $k_{\perp} = 0$ yield. In that case the tiny signal (≈ 1 mb/GeV^2) of the coherent pion radiation could be resolved from the background. The relevant spectra at several energies down to 200

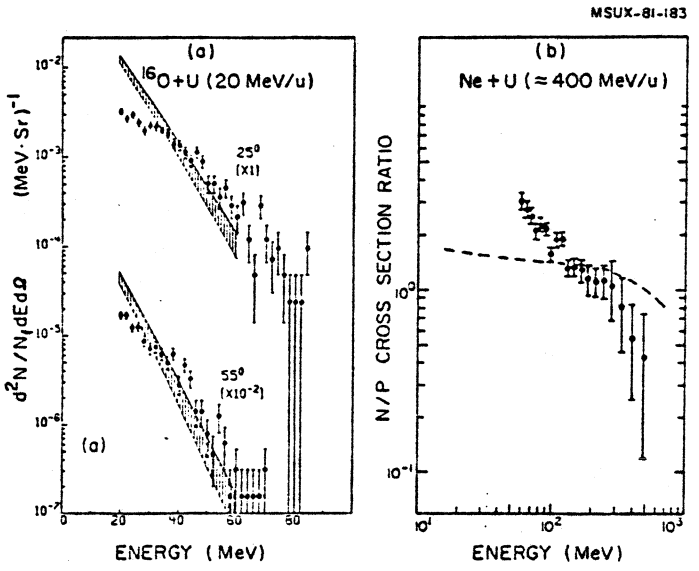

Fig. 26 (a) Differential proton multiplicities per fission event for the reaction ^{16}O + U at 20 MeV/nucleon, compared with corresponding neutron multiplicity (shaded area); (b) ratio of neutron to proton cross sections in reactions of Ne + U at ≈400 MeV/nucleon. The dashed line is the firestreak prediction.

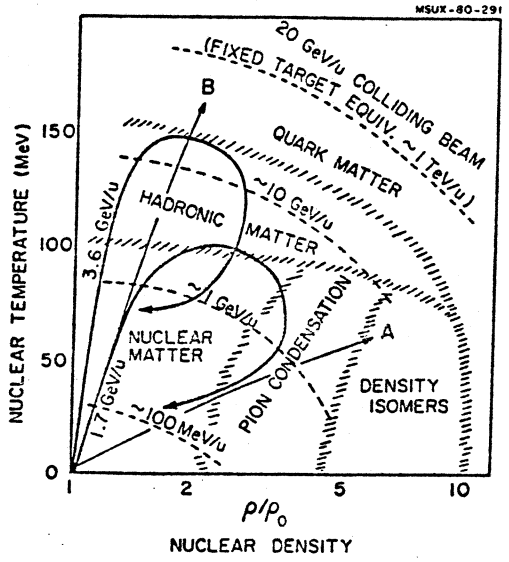

Fig. 27 Possible phases of nuclear and hadronic matter as a function of temperature and density. The T and ρ values predicted in cascade calculations of heavy-ion collisions at 3.6 and 1.7 GeV/nucleon are shown by the time trajectories.

MeV/nucleon Ne + NaF are shown[106]) in Fig. 28. At the lowest energy the predicted pionic instability (dotted line) should be clearly visible above the thermal background. In these preliminary data, there is no sign of a deviation. By going to still lower energies, e.g. 100 MeV/nucleon, the temperature, according to Fig. 4, will drop to about 20 MeV and even more sensitive limits on instabilities could be set although the limits from Fig. 28 are already very low.

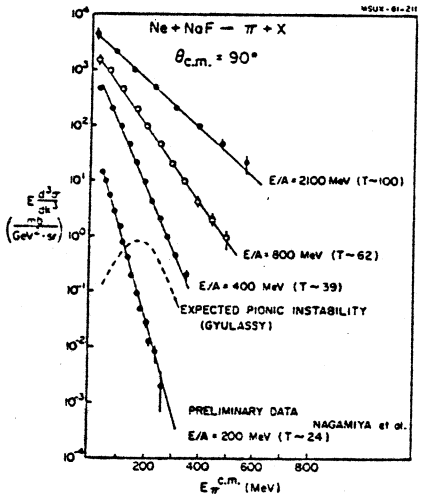

Fig. 28 Invariant pion production cross at 90° in the center of mass as a function of E_{cm} for the reaction Ne + NaF at incident energies of 2100, 800, 400 and 200 MeV/nucleon. The estimated deviation from the statistical background due to a coherent pion instability is shown by the dashed line for the 200 MeV/nucleon data.

In nucleon-nucleon collisions the threshold energy for pion production is 290 Mev. Therefore, any production in nuclear collisions below this energy is due to nuclear effects; an example is the 200 MeV/nucleon data in Fig. 28. Both π^+ and π^- emission at zero degrees has already been observed in Ne + NaF collisions at beam energies as low as 80 MeV/nucleon,[107]) as shown in Fig. 29. In the absence of any Fermi motion the creation of 70-80 MeV pions in the laboratory frame with beams of 80 MeV/nucleon, requires about 9 nucleons to sum their kinetic energies. Thus in the center of the main frame, the kinetic energy and rest mass of one of these pions is about 185 MeV, whereas the beam energy is only 20 MeV/nucleon. On the other hand if the pions are created in single nucleon-nucleon collisions, a Fermi momentum of 400 MeV/c is required. So far no satisfactory explanation of the data exist. Perhaps there is some collective enhancement at work,[106]) but to be sure the results of new theoretical trials in progress are awaited.

Another interesting effect can be seen in the data of Fig. 29. The yields of π^- are much higher than those of π^+; at certain momenta the spectra have peaks and valleys respectively (see the 383 MeV/ nucleon results). The pion velocity at this point is very close to the

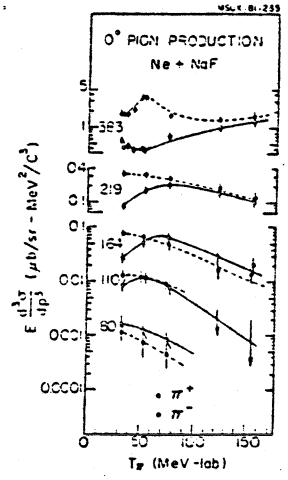

Fig. 29 Pion spectra at 0° in low energy Ne + NaF collisions.

beam velocity. It is thought that negative pions are attracted to the positively charged beam fragments, whereas the positive pions are repelled. It has also been conjectured that pionic nuclei are created.[108] However theoretical calculations with Coulomb interactions appear to explain the effect reasonably well.[109,110]

All hope is not yet lost for new phases of nuclear matter. A whole arsenal of experimental methods is being brought to bear on the problem. For example, light particle production may offer a means of determining the entropy created in the source. An excess of entropy over that produced by normal processes would indicate other degrees of freedom, such as might come about from a phase transition to a pion condensate or to quark matter.[111] It has been suggested that the deuteron to proton ratio might convey information about the entropy in the initial, hot participant zone.[111] According to recent calculations,[112,113] the subsequent hydrodynamic expansion of the zone creates little additional entropy, of the order of 0.5 units. The ratio of deuterons to protons reaching the detectors from the final phase of the reaction, where the deuterons are constantly forming and breaking up, can therefore measure the entropy in the initial state. A small number of deuterons points to large entropy and vice versa. The expected entropy per baryon of a Fermi gas as a function of energy/nucleon is shown[112] in Fig. 30. At low energies it has the form $S = (\pi^2/2\varepsilon_f)T$, whereas at high energies it has the variation $\ell n\ T$, characteristic of a classical gas. The variation is shown for cases of viscous (S_s) and inviscid (S_η) systems. Also shown[51] are the experimental specific entropies for the Ne + NaF system at 800 and 2100 MeV/nucleon, calculated from,

$$S = 3.95 - \ell n\frac{<d>}{<p>} .$$

More entropy is generated than can be accounted for in the calculation, a result which is also borne out by Monte Carlo cascade models.[114] The discrepancy has been attributed to the presence of other unknown degrees of freedom in the participant zone.[111] A more

recent analysis explains the excess of entropy in terms of pion production,[115]) but other hydrodynamic calculations continue to produce a discrepancy.[116])

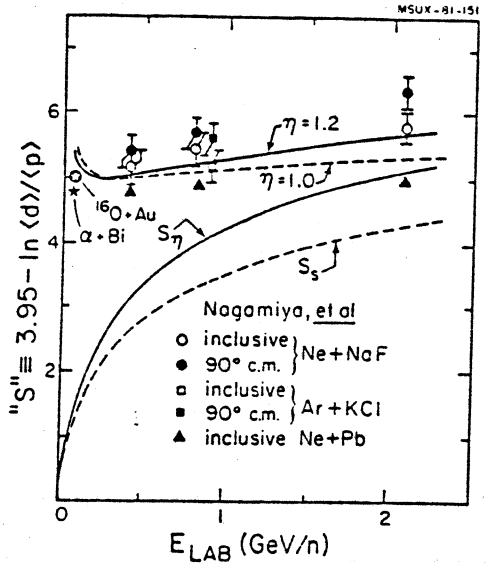

Fig. 30 Measured entropies deduced from deuteron to proton ratio for several reactions as a function of energy per nucleon. The theoretical curves are hydrodynamical predictions, discussed in the text.

A note of caution over the interpretation of this discrepancy must be injected. In Fig. 30, the function S is also plotted for data on the same system Ne + NaF at a lower energy of 400 MeV/nucleon.[51]) Here, of course, the functional form pertaining to a classical gas is not relevant, since the temperatures are low enough for Fermi and Bose statistics to act. Nevertheless, the surprising result is that the deuteron to proton ratio, and hence the function, S, derived from it, does not change very much over the entire energy range. This observation is more dramatic for the system Ne + Pb which is also shown, and can be compared with the ^{16}O + Au results at lower energies of 20 MeV/nucleon.[27]) Even data for the α + Bi system at 25 MeV/nucleon follow the trend.[117]) The uniform behaviour is apparently a feature of a hydrodynamic calculation, incorporating the decay of excited states of the light composite particles.[112]) These increase the proton population and effectively reduce the ⟨d⟩/⟨p⟩ ratio from the primary values related to the entropy. The hydrodynamical model predictions of "S", which are now no longer a direct measure of the entropy, are also shown for viscous and inviscid conditions. There are recent speculations[118]) that the deuteron to proton ratio may be limited by the exclusion principle at low energies, providing an independent explanation of the constant low energy ratio of 0.3. We should point out that the results for α + Bi, Ne + Pb and ^{16}O + Au are derived from inclusive measurements and may be contaminated by deuteron production from processes originating outside the participant

zone. Some indication of the possible contribution from non participants is shown in Fig. 29 by comparing the inclusive and the 90° cm results; the latter emphasize the intermediate rapidity fireball region. In general deuterons can be generated not only by participant - participant interactions in the fireball zone, but also be participant-spectator[119]) interaction, or by a "snowball" mechanism in which a nucleon suffers a collision and then gathers up one or more nucleons on the way out.[120])

If the above problems can be resolved, present wisdom dictates[121]) that a measurement of entropy, combined with the pressure, at low incident energies of 50-100 MeV/nucleon may offer the best hope for determining the equation of state, the latest Holy Grail of heavy-ion collisions. The reasons are summarized in Fig. 31. In part (a) the pressure and entropy, expressed relative to the values obtained in a Fermi gas in the absence of compressional effects, are plotted as a function of incident energy/nucleon for four values of the compressibility constant K, equal to 100, 200, 400 and 800 MeV. Here K is defined by $9\rho_o^2(d^2W_c/d^2\rho)$ with $W_c = K(\rho - \rho_o)^2/18\rho\rho_o$. Then $P_c(\rho)$ is just $\rho^2(dW_c/d\rho)$. Not surprisingly the greatest sensitivity is obtained at low energy. A similar comparison is made in part (b) for different functional forms of the compressional energy. In each case the thermal contribution to the pressure was fixed at $\alpha\rho W_T$ with $\alpha = 2/3$, corresponding to a Fermi gas, and $W_T = (\gamma_{cm} - 1)W_o$ with W_o the nucleon rest mass. The situation is just reversed in (c) where the compressional energy is fixed and the thermal energy is varied by setting $\alpha = 1/3$, 2/3 and 1. The greatest sensitivity to the thermal pressure and entropy is at high energies. The importance of measuring P(E) and S(E) is clear if we note that at 100 MeV/nucleon, a typical intermediate energy, it is possible to obtain identical values of P(E) for two different forms of $W_c(\rho)$ but the values of S(E) are then found to be different. It appears necessary to measure these quantities to 10% accuracy, however.

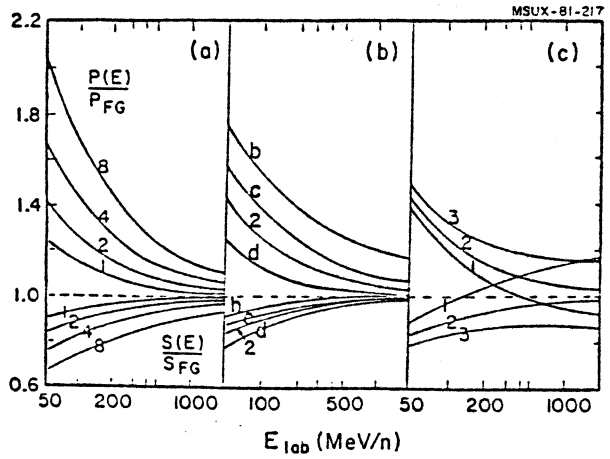

Fig. 31 Calculated pressure and entropy as a function of incident energy per nucleon expressed relative to the Fermi gas value without compression: a) compares different nuclear compressibilities; b) different equations of state and c) different thermal components.

This is a formidable requirement, given that at present there is not even any numerical value of P extracted from experimental data, and that the differences in theoretical estimates of S vary by many tens of percent! Nor is it yet clear that hydrodynamics applies for certain to any substantial part of the interaction region. Nevertheless the course has been set and the terrain is staked out for intermediate energies. The necessary experiments will probably require complete reconstruction of events like that in Fig. 16. With complete in-plane and out-of-plane measurements, hydrodynamics makes specific predictions about jet structures[122]) of light particles, that differ considerably from the cascade model.

An experimental program[3]) at intermediate energies using a streamer chamber has already begun (see Fig. 16). In this approach, values of $\langle p_\perp \rangle$ or temperature, can be extracted without assumptions about a moving source or the correct coordinate system, by projecting the particle momentum on the plane perpendicular to the beam axis. Remarkably enough the derived value of T = 35 MeV for ^{12}C on BaI_2 at 150 MeV/nucleon fits rather well onto the systematics based on the analysis of inclusive data in the moving source framework (See Fig. 19). The complete $p_\perp$ distribution is shown in Fig. 32, before and after division by the multiplicity in the event, <M>. The bulk of the events are concentrated at $p_\perp/\langle M \rangle \approx 200$ MeV/c. At this stage one can only conjecture the reasons; a blast wave imparting an ordered collective flow is one possibility.[123,124]) In an attempt to select central collisions, the displayed events have a trigger requirement that there be less than two leading beamfragments N within ±10% of the beam velocity and inside a 5° cone. The lower left hand panel shows the dependence of $\langle p_\perp/M \rangle$ on N. The rapid drop beyond N = 2 shows that the criterion is probably a good one for the selection of events with a high degree of thermalization.

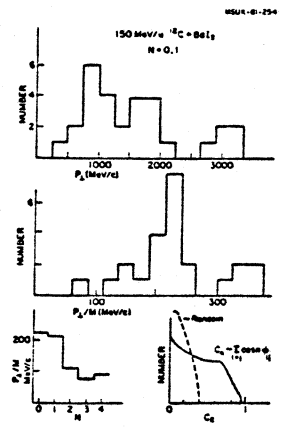

Fig. 32 Charged particle exclusive data from the Bevalac streamer chamber for p, d, t, α emitted in 150 MeV/nucleon ^{12}C + BaI_2 reactions. Top graph shows $P_\perp$ distribution in each event, which is divided by the multiplicity in the middle section; in both cases the central trigger condition of not more than one leading particle is imposed. Lower left-hand picture shows $P_\perp/M$ as function of leading particle number N. The lower right graph is an example of moment analysis of event shapes.

There is insufficient space to enter in detail on the last panel of the figure at the bottom right, important though it be. The goal is to determine event shapes associated with a number of major axes.[3,125-127]) The degree of symmetry, derived from the values of various coefficients between 0 and 1, can be compared with the predictions of different theories, e.g. hydrodynamics or TDHF. There are several schemes for making the multiparticle correlation, such as "thrust", "sphericity" and "minimum spanning tree" - concepts all borrowed from high energy physics.[128]) The derived values of one coefficient C_2 are shown and compared with the expectation in a random situation, generated by choosing tracks from different events with the same multiplicity as the events of interest. Clearly there is a large correlation effect, which comes from the presence of two jets, already visible to the eye in Fig. 16. It is hoped that this type of analysis will eventually distinguish amongst various possible explanations such as Fermi jets, which are characteristic of the mean field or long mean free path approximation, and hot spots or collective splashes, which come from the short mean free paths in hydrodynamical approaches.[129,130])

We shall end this survey with an established exotic topic that is the clear prerogative of intermediate energy nuclear collisions--that of the production of exotic nuclei. The motivation for their study is clear from the panoramic view[131]) of the stability diagram of nuclear species in Fig. 31. There are 300 or so stable nuclei in nature. During the last half century, some 1300 additional radioisotopes have been identified and studied. It is estimated that another 6000 might exist, many of which will have exotic decay modes and properties. Through the discovery of new shells, new shapes and possibly new densities these nuclei, far from stability, will subject our models of nuclear structure to new tests in which there are likely to be many surprises. This field is a rich one for spectulation. It is conjectured, for example, that nuclei of very large neutron excess might exist in which the neutrons form an expanded cloud, enveloping a conventional nucleus at the center. Such two component nuclei are not, and indeed cannot, be investigated close to the valley of stability.[132])

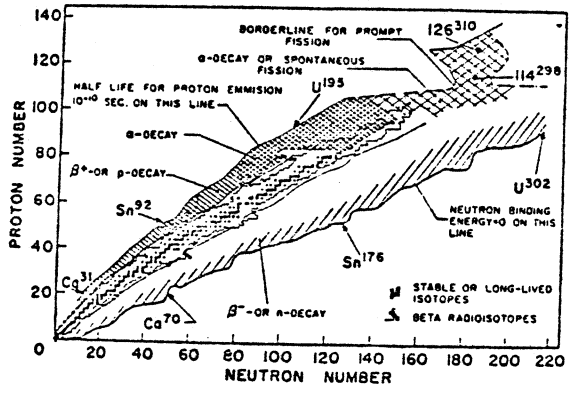

XBL 777 9479

Fig. 33 Chart of the nuclides, showing stable nuclei, known radioactive nuclei as well as theoretical limits of stability.

Intermediate energy heavy-ion beams may offer the best possibility for reaching the limits of stability in the near future, as was already clear from Fig. 11. By shearing off eight protons from ^{48}Ca it is possible to make ^{40}Mg which is predicted to be the last stable isotope of Z=12. Of course the presence of the ground state correlations, which we discussed earlier, makes it hard to remove protons alone in the high energy abrasion process, but the fact that the products are concentrated near zero degrees with small transverse momentum still makes the reaction experimentally highly efficient. The high incident energy also allows thick targets. Some twenty new isotopes have been discovered by this technique,[133-135] which are marked in Fig. 32 by the bold outlined boxes in half diagonal shading. The other diagonally shaded boxes denote nuclei discovered mainly in deep-inelastic, heavy-ion collisions.[136-139] With new accelerators, yielding beams of intermediate energy heavy ions of intensities up to ten times greater than presently available, the limits of stability of light nuclei will be reached in the near future, together with whatever surprises they contain.

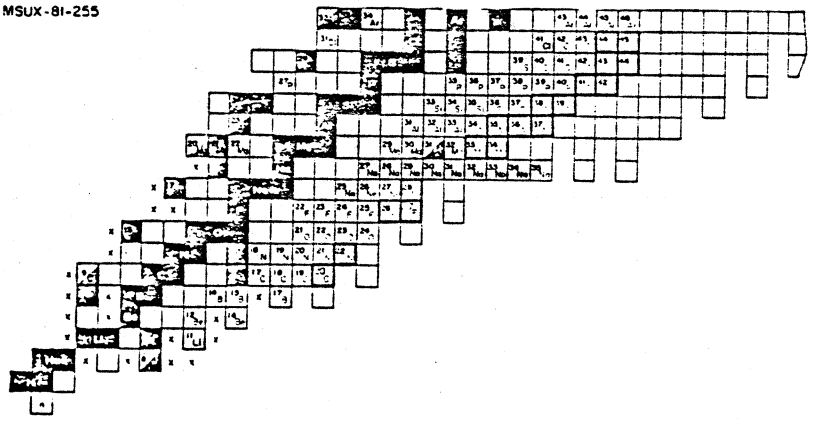

Fig. 34 Chart of nuclides showing the present status of known stable light nuclei.

From this brief survey of the current situation in intermediate energy heavy-ion collisions, it should be evident that they will be useful both in clarifying the relation between our models developed in the extremes of very low and very high energy, and in the development of new theoretical approaches. The subject is already making contributions to old problems in microscopic nuclear structure, such as the question of zero point motion, and to extending our theories of nuclear structure into new regions very far from stability. But in addition a variety of macroscopic and even exotic phenomena may find their best testing grounds at intermediate energy.[1-5]

Acknowledgements

I am grateful to T.C. Awes, G.F. Bertsch, M. Curtin, C.K. Gelbke, M. Gyulassy, B. Jacak, S. Nagamiya, P.J. Siemens, H. Stöcker, G. Westfall and K. Wolf for many useful discussions. I also thank C.K. Gelbke, M. Gyulassy, J. Natowitz, S. Nagamiya, H. Stöcker and K. Wolf for permission to use unpublished material. It is a pleasure to thank Betty Brewer and Patricia Pirnie for typing and assembling the manuscript, and M. Blosser for preparing the illustrations. The preparation of this paper was supported by the National Science Foundation under Grant No. Phy 80-17605.

†Many of the figures in the paper are redrawn from the originals for clarity. Reference to the original works should be made to obtain precise numerical values.

References

1. D.K. Scott, Nucl. Phys. A354 (1981) 375.
2. B. Jacobsson, Proc. of 4th Nordic Meeting on Intermediate and High Energy Nuclear Physics (Norway, 1981), Lund University Preprint LUIP 8102.
3. K. Wolf, Proc. of 5th High Energy Heavy Ion Study (Berkeley, 1981).
4. V.M. Galitzky and I.N. Mishustin, Proc. of Int. Conf. on Extreme States in Nuclear Systems (Dresden, 1980), ed. by H. Prade and S. Tesch, Vol. II., p. 131.
5. D.K. Scott, Proc. of Int. School on Nulcear Structure (Alushta, Crimea, 1980) ed. V. soloviev, p. 297.
6. N.J. Digiacomo, R.M. Devries and J.C. Peng, Phys. Rev. Lett. 45 (1980) 527; R.M. Devries and J.C. Peng, Phys. Rev. C22 (1980) 1055; R. Devries and J.C. Peng, Phys. Rev. Lett. 43 (1979) 1373; J.C. Peng, R.M. Devries and N. Digiacomo, Phys. Lett. 98B (1981) 244.
7. R.G. Stokstad, A.J. Cole, W.B. Rae, A. Dacal, B.G. Harvey, R. Legrain, J. Mahoney and M.J. Murphy, Abstracts of 5th High Energy Heavy Ion Study (Berkeley, 1981) LBL-12652, p. 62; A.J. Cole et al., to be published.
8. J. Jaros, A. Wagner, L. Anderson, O. Chamberlain, R.Z. Fuzesy, J. Gallup, W. Gorn, L. Schroeder, S. Shannon, G. Shapiro and H. Steiner, Phys. Rev. C18 (1978) 2273.
9. A. Gobbi and W. Norenberg in Heavy Ion Collisions, ed. R. Bock (North Holland, 1979) Vol. II, p. 129.
10. D. Glas and U. Mosel, Nucl. Phys. A237 (1975) 429.
11. G. Gregoire, C. Ngo and B. Remaud, Phys. Lett. 99B (1981) 17 and refs. therein.
12. J. Wilczynski, K. Siwek-Wilzynska, J. Van Driel, S. Gonggryp, D.C.J.M. Hageman, R.V.F. Janssens, J. Lukasiak and R.H. Siemssen, Phys. Rev. Lett. 45 (1980) 606 and refs. therein.
13. R.K. Bhomik, E.C. Pollacco, N.E. Sanderson, J.B.A. England and G.C. Morrison, Daresbury Preprint DL/NUC/P 123E (1980), to be published in Nucl. Phys. A.
14. S. Nagamiya and D.J. Morrissey, Lawrence Berkeley Laboratory Preprint, LBL-10461, 1980.
15. H. Stocker, J.A. Maruhn and W. Greiner, Phys. Rev. Lett. 44 (1980) 725.
16. J. Cugnon, Phys. Rev. C22 (1980) 1885.

17. J. Negele, Proc. of Int. Conf. on Extreme States in Nuclear Systems (Dresden, 1980), eds. H. Prade and S. Tesch, Vol. II, p. 198.
18. B. Jacobsson, L. Carlen, P. Kristiansson, H.A. Gustafsson, T. Johansson, H. Ryde, G. Tibell, J.P. Bondorf, G. Fai, A.O.T. Karvinen, O.B. Nielsen, M. Buenerd, J. Cole, D. Lebrun, J.M. Loiseaux, P. Martin, R. Ost, C. Guet, E. Monnand, J. Mougey, H. Nifenecker, P. Perring, J. Pinston, C. Ristori and F. Schussler, Phys. Lett 102 B (1981) 121.
19. R. Hagedorn and J. Rafelski in Proc. of Workshop on Future Relativistic Heavy Ion Experiments (GSI, Darmstadt, 1980), eds. R. Bock and R. Stock, GSI 81-6 (1981), p. 236 and 282.
20. N.K.Glendenning and Y. Karant, Phys. Rev. Lett. 40 (1978) 374; N.K. Glendenning, Theor. Meth. in Medium Energy and Heavy Ion Physics, eds., K.W. McVoy and W.A. Friedman (Plenum, N.Y.) (1978) p. 451.
21. J.B. Natowitz, M.N. Namboodiri, L. Adler, R.P. Schmitt, R.L. Watson, S. Simon, M. Berlanger and R. Choudhury, TAMU Preprint, 1981.
22. A.S. Goldhaber, Phys. Lett. 53B (1974) 306.
23. E.J. Moniz, I. Sick, R.R. Whitney, J.R. Ficenec, R.D. Kephart and W.P. Trower, Phys. Rev. Lett. 26 (1971) 445.
24. Ch. Egelhaff, G. Bohlen, H. Fuchs, A. Gamp, H. Homeyer and H. Kluge, Phys. Rev. Lett. 46 (1981) 813.
25. T.C. Awes, C.K. Gelbke, B.B. Back, A.C. Mignerey, K.L. Wolf, H. Breuer, V.E. Viola and W.G. Meyer, Phys. Lett. 87B (1979) 43.
26. T.C. Awes, C.K. Gelbke, G. Poggi, B.B. Back, B. Glagola, H. Breuer, V.E. Viola and T.J.M. Symons, Phys. Rev. Lett. 45 (1980) 513.
27. T.C. Awes, G. Poggi, C.K. Gelbke, B.B. Back, B.G. Glagola, H. Breuer and V.E. Viola, Michigan State University Preprint MSUCL-343 (1980).
28. U. Lynen, Private communication (1980).
29. F. Saint-Laurent, M. Conjeaud, R. Dayras, S. Harar, C. Volant and H. Oeschler, Proc. of Versailles Conf. (1981).
30. K. Swiek-Wilczynska, E.H. du Marchie van Vorthuysen, J. Van Popta, R.H. Siemssen and J. Wilczynski, Phys. Rev. Lett. 42 (1979) 1599.
31. This feature was pointed out to me by K. Wolf.
32. S. Sandoval, H.H. Gutbrod, W.G. Meyer, A.M. Poskanzer, R. Stock, J. Gosset, J.-C. Jourdain, C.H. King, C. King, Ch. Lukner, Nguyen Van Sen, G. Westfall and K.L. Wolf, Phys. Rev. C 21 (1980) 1321.
33. J. Gosset, J.I. Kapusta and G.D. Westfall, Phys. Rev. C 18 (1978) 844.
34. F.S. Hernandez and G. Mantzouranis, Phys. Rev. C22 (1980) 575.
35. J. Hufner and M.C. Nemes, Phys. Rev. C23 (1981) 2538.
36. Y.P. Viyogi, T.J.M. Symons, P. Doll, D.E. Greiner, H.H. Heckman, D.L. Hendrie, P.J. Lindstrom, D.K. Scott, K. Van Bibber and G.D. Westfall, Phys. Rev. Lett. 42 (1979) 33.
37. G. Bertsch, Phys. Rev. Lett 46 (1981) 472.
38. J.B. Bondorf, G. Fai and O.B. Nielson, Phys. Rev. Lett. 41 (1978) 391.
39. D.J. Morrissey, Proc. of Symp. on Heavy Ion Physics from 10 to 200 MeV/nucleon (1979), Brookhaven National Laboratory Report BNL-51115, p. 821.
40. G.D. Westfall, private communication 1980; Y.P. Viyogi et al., to be published.
41. X. Campi and J. Hufner, Preprint, 1981.

42. D.E. Greiner, P.J. Lindstrom, H.H. Heckman, B. Cork and F. Beiser, Phys. Rev. Lett. 35 (1975) 152.
43. K. Van Bibber, D.L. Hendrie, D.K. Scott, H.H. Wieman, L.S. Schroeder, J.V. Geaga, S.A. Chessin, R. Truehaft, J.Y. Grossiord, J.O. Rasmussen and C.Y. Wong, Phys. Rev. Lett. 43 (1979) 840.
44. R. Legrain, T.C. Awes, H.J. Crawford, C.K. Gelbke, D.E. Greiner, H.H. Heckman, J.M. Kidd, P.J. Lindstrom, J. Mahoney, D.K. Scott, T.J.M. Symons and G.D. Westfall, Proc. of Int. Conf. on Nucl. Phys. (Berkeley, 1980), Abstracts, Lawrence Berkeley Laboratory Report LBL-11118, p 532.
45. J. Mougey, R. Ost, M. Buenerd, A.J Cole, C. Guet, D. Lebrun, J.M. Loiseaux, P. Martin, M. Maurel, E. Monnand, H. Niefenecker, P. Perrin, J. Pinston, C. Ristori, P. de Saintignon, F. Schussler, L. Carlen, B. Jakobsson, A. Oskarsson, I. Otterlund, B. Schroder, H.A. Gustafsson, T. Johansson, H. Ryde, J.P. Bondorf, O.B. Nielsen and G. Tibell, Preprint 1981, to be published in Phys. Lett. B.
46. C.M. Ko, Phys. Rev. C 21 (1980) 2672.
47. H. Stocker, J.A. Maruhn and W. Greiner, Z. Phys. A293 (1979) 173.
48. H. Stocker, R.Y. Cusson, J.A. Maruhn and W. Greiner, Phys. Lett. 101B (1981) 379.
49. C.Y. Wong, Proc. of Symp. on Heavy Ion Physics from 10 to 200 MeV/nucleon, Brookhaven National Laboratory Report BNL-51115, p. 329.
50. T.C. Awes, G. Poggi, S. Saini, C.K. Gelbke, R. Legrain and G.D. Westfall, Michigan State University Preprint MSUCL-351 (1981), to be published in Phys. Lett. B.
51. S. Nagamiya, M.-C. Lemaire, E. Moeller, S. Schnetzer, G. Shapiro, H. Steiner and I. Tanihata, Lawrence Berkeley Laboratory Preprint LBL-12123, 1981 and to be published in Phys. Rev. C.
52. J. Gosset, H.H. Gutbrod, W.G. Meyer, A.M. Poskanzer, A. Sandoval, R. Stock and G.D. Westfall, Phys. Rev. C 16 (1977) 629.
53. W.D. Myers, Nucl. Phys. A 296 (1978) 177.
54. S. Das Gupta, Phys. Rev. C 18 (1978) 2773.
55. J. Cugnon, Phys. Rev. C 22 (1980) 1885.
56. K.R. Cordell, S.T. Thornton, L.C. Dennis, R.R. Doering, R.L. Parks and T.C. Schweizer, Nucl. Phys. A 362 (1981) 431.
57. H.C. Chiang and J. Hufner, Nucl. Phys. A349 (1980) 466.
58. J. Cugnon, Phys. Rev. C 23 (1981) 2094.
59. M. Chemtob and B. Schurmann, Nucl. Phys. A336 (1980) 508.
60. B. Schurmann, K.M. Hartmann and H.J. Pirner, Nucl. Phys. A360 (1981) 435.
61. B. Schurmann and J. Randrup, Phys. Rev. C 23 (1981) 2766.
62. For further discussion, see D.K. Scott, Michigan State University Preprint MSUCL-355, to be published in Proc. of Topical Conf. on Dynamical Properties of Heavy Ion Collisions, Hvar, 1981.
63. M.T. Collins and J.J. Griffin, Nucl. Phys. A 34 (1980) 863.
64. J.W. Negele and K. Yazaki, Phys. Rev. Lett. 47 (1981) 71.
65. S.I.A. Garpman, D. Sperber and M. Zielinska-Pfabe, Nuov. Cim. 57B (1980); K. Muller, Phys. Lett. 93B (1980) 247.
66. P.A. Gottschalk and M. Westrom, Nucl. Phys. A314 (1979) 232.
67. R. Weiner and M. Westrom, Nucl. Phys. A256 (1977) 282.
68. R.M. Weiner, Phys. Rev. D 13 (1976) 1363; Phys. Rev. Lett. 32 (1974) 630.
69. H. Ho, R. Albrecht, W. Dunnweber, G. Graw, S.G. Steadman, J.P. Wurm, D. Disdier, V. Rauch and F. Schiebling, Z. Phys. A283 (1977) 235.

70. J. Goldberg, Phys. Rev. Lett. 43 (1979) 250.
71. R. Weiner, Proc. of Int. Workshop on Reaction Models for Continuous Spectra of Light Particles, Bad Honnef, 1978, edited by J. Ernst.
72. W.W. Morison, S.K. Samaddar, D. Sperber and M. Zielinska-Pfabe, Phys. Lett. 93B (1980) 279 and refs. therein.
73. P. Mooney, W.W. Morison, S.K. Samaddar, D. Sperber and M. Zielinska-Pfabe, Phys. Lett. 98B (1981) 240.
74. J.P. Bondorf, Proc. of Conf. on Large Amplitude Nuclear Motion, Lake Balaton (1979) p. 482.
75. W.A. Friedman and P. Saloner, Phys. Rev. C23 (1981) 2532 and refs. therein.
76. W. Dunnweber and K.M. Hartmann, Phys. Rev. Lett. 44 (1980) 729.
77. H. Ho, P. Gonthier, M.N. Namboodiri, J.B. Natowitz, L. Adler, S. Simon, K. Hagel, R. Terry and A. Khodai, Phys. Rev. Lett. 44 (1980) 1387.
78. M. Bini, C.K. Gelbke, D.K. Scott, T.J.M. Symons, P. Doll, D.L. Hendrie, J.L. Laville, J. Mahoney, M.C. Mermaz, C. Olmer, K. Van Bibber and H.H. Wieman, Phys. Rev. C 22 (1980) 1945.
79. N.S. Wall, J.R. Wu, G.C. Chang and H.D. Holmgren, Phys. Rev. C 20 (1979) 1079.
80. N. Stelte and R.M. Weiner, Proc. of XX Int. Conf. on High Energy Physics, Madison, 1980.
81. C.M. Ko and M. Ta-Chung, Phys. Rev. Lett. 43 (1979) 994.
82. R.H. Landau and M. Gyulassy, Phys. Rev. C 19 (1979) 149.
83. M.C. Lemaire, S. Nagamiya, S. Schnetzer, H. Steiner and I. Tanihata, Phys. Lett. 85B (1979) 38.
84. A. Mekjian, Phys. Rev. Lett. 38 (1977) 640; Phys. Rev. C 17 (1978) 1051; Phys. Lett. 89B (1980) 177.
85. B.K. Jennings, S. Das Gupta and N. Mobed, Preprint 1981.
86. S. Das Gupta and A. Mekjian, Phys. Reports, to be published.
87. H. Sato and K. Yazaki, Phys. Lett. 98B (1981) 153.
88. G. Gaul, R. Glasow, H. Lohner, B. Ludewight and R. Santo, private communication; H. Lohner, B. Ludewigt, D. Frekers, G. Gaul and R. Santo, Z. Phys. A292 (1979) 35.
89. H. Machner, Phys. Rev. C 21 (1980) 2695; Phys. Lett. 96B (1979) 129.
90. S.Y. Fung, W. Gorn, G.P. Kiernan, J.J. Lu, T.Y. Oh and R.T. Poe, Phys. Rev. Lett. 41 (1978) 1592.
91. J. Bartke, Proc. of the Int. Conf. on Nuclear Physics (abstracts), Lawrence Berkeley Laboratory Reprot LBL-11118, p. 537.
92. F. Zarbakhsh, A.L. Sagle, F. Brouchard, T.A. Mulera, V. Perez-Mendez, R. Talaga, I. Tanihata, J.B. Carroll, K.S. Ganzer, G. Igo, J. Oostens, D. Woodward and R. Sutter, Phys. Rev. Lett. 46 (1981) 1268.
93. M. Gyulassy, S.K. Kauffmann and L. Wilson, Phys. Rev. C 20 (1979) 2267.
94. S.I.A. Garpman, S.K. Samaddar, D. Sperber and M. Zielinska-Pfabe, Phys. Lett. 92B (1980) 56.
95. H.H.K. Tang and C.Y. Wong, Phys. Rev. C 21 (1980) 1846.
96. G.F. Bertsch and P.J. Siemens, private communication, 1981.
97. K.A. Frankel and J.D. Stevenson, Phys. Rev. 23 (L981) 1511.
98. J. Randrup and S.E. Koonin, Nucl. Phys. A356 (1981) 223.
99. E. Fermi, Prog. Th. Phys. 5 (1950) 570.
100. J. Stevenson, P.B. Price and K. Frankel, Phys. Rev. Lett. 38 (1977) 1125.
101. W. Schimmerling, J.W. Kast, D. Orthendahl, R. Madey, R.A. Cecil, B.D. Anderson and A.R. Baldwin, Phys. Rev. Lett. 43 (1979) 1985; J.D. Stevenson, Phys. Rev. Lett. 45 (1980) 1773.

102. J.D. Stevenson, Lawrence Berkeley Laboratory Preprint LBL-11736 (1980).
103. J. Kasagi, S. Saini, T.C. Awes, A. Galonsky, C.K. Gelbke, G. Poggi, D.K. Scott, K.L. Wolf and R. Legrain, Michigan State University Preprint MSUCL-352 (1981), to be published in Phys. Lett. B.
104. Adapted from K.K. Gudima and V.D. Toneev, Dubna JINR-Preprint E2-12624 (1979).
105. See, for example, M. Gyulassy, Nucl. Phys. A354 (1981) 395.
106. S. Nagamiya, Proc. of 5th High Energy Heavy Ion Study (Berkeley, 1981), LBL Preprint 12950; M. Gyulassy, private communication, 1981.
107. W. Benenson, G. Bertsch, G.M. Crawley, E. Kashy, J.A. Nolen, H. Bowman, J.G. Ingersoll, J.O. Rasmussen, J. Sullivan, M. Koike, J. Peter and T.E. Ward, Phys. Rev. Lett. 43 (1979) 683.
108. P.J. Siemens and C.M. Ko, Nucl. Phys. A367 (1981) 496.
109. K.G. Libbrecht and S.E. Koonin, Phys. Rev. Lett. 43 (1979) 581.
110. M. Gyulassy and S.K. Kauffmann, Nucl. Phys. A362 (1981) 503.
111. P.J. Siemens and J.I. Kapusta, Phys. Rev. Lett. 43 (1979) 1486.
112. H. Stock, Lawrence Berkeley Laboratory Preprint LBL-12302 (1981).
113. L.P. Csernai and H.W. Barz, Z. Phys. A296 (1980) 1.
114. G.F. Bertsch and J. Cugnon, Proc. of 5th High Energy Heavy Ion Summer Study (Berkeley, 1981).
115. I.N. Mishustin, F. Myhrer and P.J. Siemens, Phys. Lett. 95B (1980) 361.
116. J.I. Kapusta and D. Strottman, Phys. Rev. C 23 (1981) 1282.
117. J.R. Wu, G.C. Chang and H.D. Holmgren, Phys. Rev. C 19 (1979) 659.
118. P.J. Siemens, private communication, 1981.
119. F. Hachenberg, H.C. Chiang and J. Hufner, Phys. Lett. 97B (1980) 183.
120. D.H. Boal and M. Soroushian, Preprint TRI-PP-81-7 (1981).
121. H. Stocker, M. Gyulassy and J. Boguta, Lawrence Berkeley Laboratory Preprint, LBL-12095 (1981).
122. H. Stocker, L.P. Csernai, G. Graebner, G. Buchwald, H. Kruse, R.Y. Cusson, J.A. Maruhn and W. Greiner, Lawrence Berkeley Laboratory Preprint, LBL-11774 (1981).
123. H. Stocker, in Proc. of Int. Conf. on Extreme States in Nuclear Systems (Dresden, 1980), eds. H. Prade and S. Tesch, p. 23.
124. P.J. Siemens and J.O. Rasumssen, Phys. Rev. Lett. 42 (1979) 880.
125. R. Stock, Proc. of 5th High Energy Heavy Ion Study (Berkeley, 1981), to be published.
126. C.Y. Wong, Phys. Lett. 88B (1979) 39.
127. G.F. Bertsch and A.A. Amsden, Phys. Rev. C 18 (1978) 1293.
128. G.C. Fox and S. Wolfram, Phys. Rev. Lett. 41 (1978) 1581.
129. L.P. Csernai and W. Greiner, Phys. Lett 99B (1981) 85.
130. P.J. Siemens, Proc. of Hakone Seminar on High Energy Nuclear Interactions and Properties of Dense Nuclear Matter, eds K. Nakai and A.S. Goldhaber, 1980, Vol. I, p. 306.
131. D.A. Bromley, Proc. Int. Conf. on Nucl. Phys. (Munich 1973), eds. J. de Boer and H.J. Mang (North Holland, 1973) p. 21.
132. D.H. Wilkinson, Proc. of 3rd Int. Conf. on Nuclei far from Stability (Cargese) CERN Report 76-13, p. 71.; C.Y. Wong, Proc. of Int. Conf. on Superheavy Elements, (Lubbock, Texas) Ed. M.A.K. Lodhi (Pergamon) p. 524.
133. T.J.M. Symons, Y.P. Viyogi, G.M. Westfall, P. Doll, D.E. Greiner, H. Faraggi, P.J. Lindstrom, D.K. Scott, H.J. Crawford and C. McParland, Phys. Rev. Lett. 42 (1979) 40.

134. G.D. Westfall, T.J.M. Symons, D.E. Greiner, H.H. Heckman, P.J. Lindstrom, J. Mahoney, A.C. Shotter, D.K. Scott, H.J. Crawford, C. McParland, T.C. Awes, C.K. Gelbke and J.M. Kidd, Phys. Rev. Lett. 43 (1979) 1859.
135. J.D. Stevenson and P.B. Price, Lawrence Berkeley Laboratory Preprint LBL-11737 (1980).
136. H. Breuer, K.L. Wolf, B.G. Glagola, K.K. Kwiatowski, A.C. Mignerey, V.E. Viola, W.W. Wilcke, W.U. Schroder, J.R. Huizenga, D. Hilscher and J. Birkelund, Phys. Rev. C22 (1980) 2454.
137. D. Guerreau, J. Galin, B. Gatty, X. Tarrago, J. Girard, R. Lucas and C. Ngo, Z. Phys. A 295 (1980) 105.
138. P. Auger, T.H. Chiang, J. Galin, B. Gatty, D. Guerreau, E. Nolte, J. Pouthas, X. Tarrago and J. Girard, Z. Phys. A289 (1979) 255.
139. V.V. Volkov, Phys. Reports 44 (1978) 93 and refs. therein.